COLLISIONAL BROADENING OF THE DEPOLARIZED RAYLEIGH AND ROTATIONAL RAMAN LINES IN GASES

R. A. J. KEIJSER

STELLINGEN

I

Rowell, Aval and Barrett gebruiken ten onrechte de klassieke lichtverstrooiingstheorie bij de berekening van de intensiteitsverdeling in het Ramanspectrum van H_2.

Rowell, R.L., Aval, G.M. en Barrett, J.J., J. Chem. Phys. *54* (1971) 1960.

II

Bij de beschrijving van de brekingsindex in het kritische gebied wordt, bij het afschatten van de termen van verschillende orde in de polarisatiedichtheid, te weinig rekening gehouden met het dispersieve karakter van deze termen.

Larsen, S.Y., Mountain, R.D. en Zwanzig, R., J. Chem. Phys. *42* (1965) 2187.
Hocken, R. en Stell, G., Phys. Rev. A *8* (1973) 887.

III

Voor paramagnetische kristallen met een anisotrope g-factor is het in bepaalde gevallen mogelijk $g_\perp$ te bepalen uit metingen van de spin-spin relaxatietijd.

IV

In foton echo experimenten zoals beschreven door Schmidt, Berman en Brewer kunnen snelheidsveranderende botsingen ook een rol van betekenis spelen in de relaxatietijd T_1.

Schmidt, J., Berman, P.R. en Brewer, R.G., Phys.Rev. Letters *31* (1973) 1103.

V

De verklaring die Clough geeft voor het optreden van een dipolaire polarisatie in γ-picoline kan op eenvoudige wijze getest worden.

Clough, S., Phys. Letters *42A* (1973) 371.

VI

Ten onrechte trekken Collins en Kemp uit de door hen gepresenteerde gegevens voor Germanium thermometers de conclusie dat een polynoomaanpassing niet geschikt is voor het vastleggen van het verband tussen weerstand en temperatuur.

Collins, J.G. en Kemp, W.R.G., Temperature, its Measurement and Control in Science and Industry (Instrum. Soc. of America, Pittsburg, 1972) Vol. 4, Part 2.

VII

Hoewel resonante energieoverdracht niet bijdraagt tot rotatie-translatie relaxatie, kan het effect van quasi-resonante botsingen zeer aanzienlijk zijn.

Dit proefschrift, hoofdstuk III.

VIII

De manier waarop Hess de opsplitsing van de gedepolariseerde Rayleighlijn in een magnetisch veld behandelt wekt ten onrechte de indruk dat voor O_2 en NO een splitsing in maximaal 5 componenten optreedt.

Hess, S., Springer Tracts Mod. Phys. *54* (1970) 136.

IX

Bij botsingsexperimenten met een moleculaire bundel bestaande uit meeratomige moleculen dient men er rekening mee te houden dat in de primaire bundel polarisatie effecten op kunnen treden.

X

Op grond van de uitkomsten van hoofdstuk I van dit proefschrift moet men verwachten dat resultaten van stromings dubbele breking experimenten in gassen niet op eenvoudige wijze in verband gebracht kunnen worden met resultaten voor het viscomagnetisch effect.

Baas, F., Phys. Letters *36A* (1971) 107.

XI

Aan de hand van de resultaten van de "close-coupling" berekeningen van Shafer en Gordon voor de verbreding van de gedepolariseerde Rayleighlijn voor het systeem H_2-He kan geconcludeerd worden dat de "distorted wave Born approximation" voor dit systeem geen bevredigende beschrijving geeft.

Shafer, R. en Gordon, R.G., J. Chem. Phys. *58* (1973) 5422.
McCourt, F.R., Rudensky, T. en Moraal, H., Can. J. Phys. *51* (1973) 1627.

XII

Voor vakgebieden waarin wetenschappelijke ontwikkelingen een direct economisch belang hebben is het nut van wetenschappelijke conferenties twijfelachtig.

R.A.J. Keijser

Leiden, 12 december 1973

COLLISIONAL BROADENING OF THE DEPOLARIZED RAYLEIGH AND ROTATIONAL RAMAN LINES IN GASES

PROEFSCHRIFT

TER VERKRIJGING VAN DE GRAAD VAN DOCTOR IN DE WISKUNDE EN NATUURWETENSCHAPPEN AAN DE RIJKSUNIVERSITEIT TE LEIDEN, OP GEZAG VAN DE RECTOR MAGNIFICUS DR. A. E. COHEN, HOOGLERAAR IN DE FACULTEIT DER LETTEREN, VOLGENS BESLUIT VAN HET COLLEGE VAN DEKANEN TE VERDEDIGEN OP WOENSDAG 12 DECEMBER 1973 TE KLOKKE 14.15 UUR.

DOOR

ROBERTUS ANTONIUS JOHANNES KEIJSER
GEBOREN TE RIJSWIJK (ZH) IN 1945

1973
DRUKKERIJ J. H. PASMANS, 'S-GRAVENHAGE

Promotor: Dr. H.F.P. KNAAP

Aan mijn ouders

Aan Trees

Het in dit proefschrift beschreven onderzoek werd uitgevoerd als onderdeel van het programma van de werkgemeenschap voor Molecuulfysica van de Stichting voor Fundamenteel Onderzoek der Materie (F.O.M.) met financiele steun van de Nederlandse Organisatie voor Zuiver Wetenschappelijk Onderzoek (Z.W.O.).

CONTENTS

INTRODUCTION

When a beam of light passes through a gas a small fraction of the light will be scattered in all directions. The basic principles of this phenomenon have long been known but there has been a growing interest in this field over the last decade. This development is closely connected with the introduction of the laser some ten years ago. With the monochromatic, intense, and highly collimated light of a laser beam, light scattering experiments can be carried out with a much higher precision than with conventional light sources. Moreover, it has become possible to study several aspects of light scattering that could not be investigated before.

In this introduction we summarize some of the most important characteristics of light scattering in gases. In particular those aspects are discussed that are essential for the experimental study presented in this thesis.

1. Polarization and spectral distribution of the scattered light. Let us consider the scattering of a monochromatic, linearly polarized beam of light, incident on a gas sample. The incident light is characterized by an electric field vector $\underline{E}_0$ and a frequency ν_0. The scattered light, denoted by the quantities $\underline{E}$ and ν, is studied in a direction perpendicular to $\underline{E}_0$.

First a qualitative discussion of the polarization of the scattered light is given. For spherical molecules, *e.g.* monatomics, the situation is quite simple. Since the polarizability α of a spherical molecule is isotropic, the incident light induces oscillating dipoles $\underline{\mu}_{ind}$, parallel to the electric field $\underline{E}_0$ acting on the molecules. The radiation from such a dipole is polarized in the plane defined by the dipole itself and the direction of propagation. As a consequence, the scattered light will be linearly polarized parallel to $\underline{E}_0$ (see fig. 1).

For nonspherical particules the situation is essentially different, as can be best illustrated with the example of a linear molecule. Such a linear molecule is characterized by a polarizability $\alpha_{/\!/}$ along the internuclear axis and polarizability $\alpha_{\perp}$ $(\neq \alpha_{/\!/})$ in a direction perpendicular

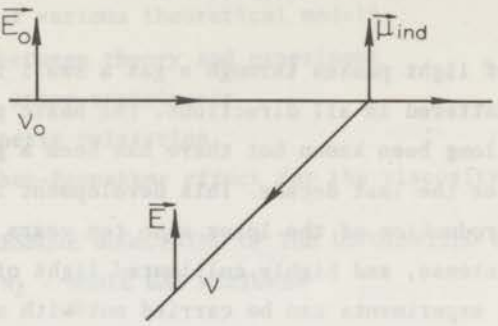

Fig. 1. Light scattering by spherical molecules.

to that axis (see fig. 2). The direction of a dipole, induced by the incident light, depends in this case on the orientation of the molecule and is in general not parallel to $\underline{E}_0$. Consequently, the scattered light is partly depolarized, *i.e.*, it contains a component E_{depol} ($\perp \underline{E}_0$), in addition to the polarized component E_{pol} ($/\!/ \underline{E}_0$) (see fig. 3).

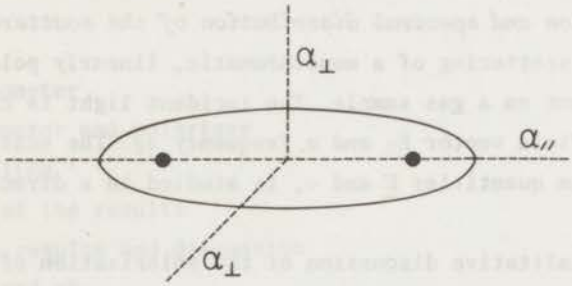

Fig. 2. The polarizability of a linear molecule.

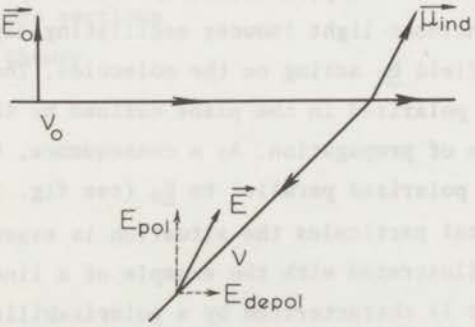

Fig. 3. Light scattering by linear molecules.

In light scattering experiments on gases the number of scattering particles is usually large and the interparticle separation is small compared to the wavelength λ of the light. The scattering of light in this case is governed by local fluctuations of the dielectric constant, which in general has the form of a second rank tensor: $\underline{\underline{\varepsilon}}$ [1]. This has been the starting point for the development of a kinetic theory of light scattering by gases of linear, nonpolar molecules by Hess[2,3]. When the gas is dilute, each molecule is unaffected by its surroundings so that the instantaneous induced polarization $\underline{P}$, due to an electric field $\underline{E}_0$, can be written in terms of the molecular polarizability tensor $\underline{\underline{\alpha}}$:

$$\underline{P} = n \langle \underline{\underline{\alpha}} \rangle \cdot \underline{E}_0 \quad . \tag{1}$$

The brackets $\langle\ \rangle$ indicate a local, instantaneous average over the one particle distribution function and n is the local number density of the gas. Both n and $\langle \underline{\underline{\alpha}} \rangle$ fluctuate in space and time.
With $\underline{D} = \underline{E}_0 + 4\pi \underline{P} = \underline{\underline{\varepsilon}} \cdot \underline{E}_0$ one obtains the relation

$$\underline{\underline{\varepsilon}} - \underline{\underline{U}} = 4\pi n \langle \underline{\underline{\alpha}} \rangle \ , \tag{2}$$

with $\underline{\underline{U}}$ the unit second rank tensor. For linear molecules the polarizability tensor $\underline{\underline{\alpha}}$ can be decomposed into an isotropic (scalar) part depending only on the average polarizability $\bar{\alpha} = \frac{1}{3}(2\alpha_\perp + \alpha_{/\!/})$ and an anisotropic (symmetrical) part depending on $(\alpha_{/\!/} - \alpha_\perp)$:

$$\underline{\underline{\alpha}} = \bar{\alpha}\, \underline{\underline{U}} + (\alpha_{/\!/} - \alpha_\perp)\, \overline{\underline{u}\underline{u}} \quad . \tag{3}$$

The quantity $\overline{\underline{u}\underline{u}}$ is a symmetric traceless tensor given by

$$\overline{\underline{u}\underline{u}} = \underline{u}\underline{u} - \frac{1}{3}\underline{\underline{U}} \ , \tag{4}$$

where $\underline{u}$ is a unit vector along the internuclear axis. If one assumes $\alpha_{/\!/}$ and $\alpha_\perp$ to be constant (the rigid rotator approximation), eq. (2) can

be written in the form

$$\underline{\underline{\varepsilon}} - \underline{\underline{U}} = 4\pi n\bar{\alpha}\,\underline{\underline{U}} + 4\pi n\,(\alpha_{/\!/} - \alpha_{\perp})\,\langle\overline{\underline{u}\underline{u}}\rangle \quad . \qquad (5)$$

The first term on the right hand side of eq. (5) is isotropic and produces so-called scalar scattering via fluctuations in the number density n. This scattering is polarized parallel to $\underline{E}_0$ and appears in the spectrum centered around the exciting frequency ν_0. In general it has the form given in fig. 4 and is known as the Rayleigh-Brillouin triplet.

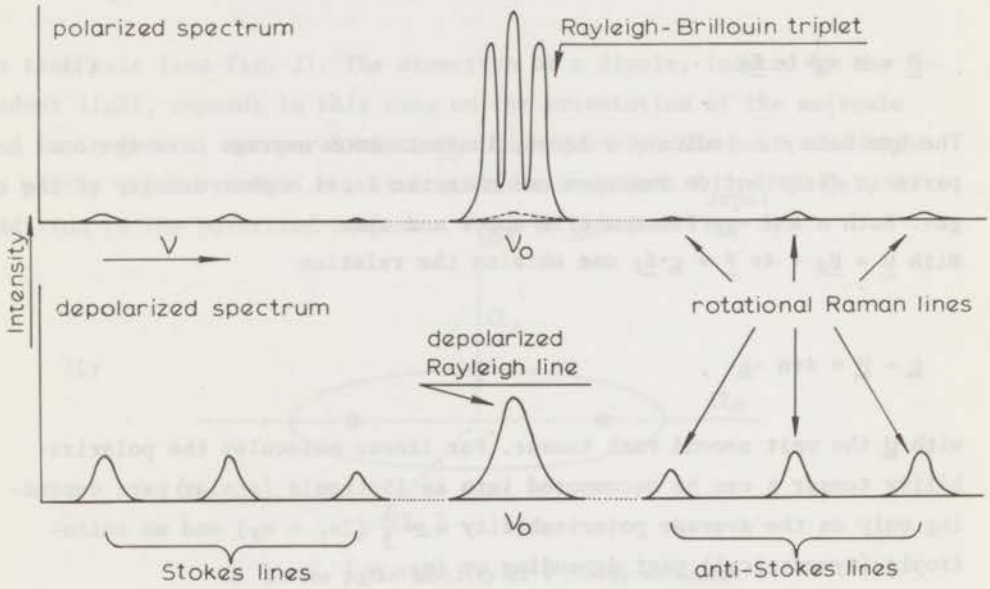

Fig. 4. Spectrum of the polarized and depolarized scattered light. This diagram is only schematic, the intensity in the depolarized spectrum being typically 1% of the polarized intensity.

Usually this triplet contains the major part of the scattered intensity. The second term in eq. (5) is anisotropic and produces both polarized and depolarized scattering via fluctuations in $\langle\overline{\underline{u}\underline{u}}\rangle$, *i.e.*, fluctuations in the molecular orientations. This scattering is known as symmetrical or anisotropic scattering. The tensor operator $\overline{\underline{u}\underline{u}}$ contains a part diagonal in the rotational quantum number j and further nondiagonal parts $(\overline{uu})^{jj'}$, which are nonzero for $j' = j \pm 2$. The selection

rule for symmetrical scattering is thus $\Delta j = 0, \pm 2$. The unshifted component, corresponding to $\Delta j = 0$, is, in the polarized spectrum, hidden under the intense Rayleigh-Brillouin triplet, but in the depolarized spectrum it appears as a well resolved line, the *depolarized Rayleigh line*, The lines corresponding to transitions between the rotational states of the molecules ($\Delta j = \pm 2$) appear as series of equidistant lines in both polarized and depolarized spectrum. They are known as the *rotational Raman lines*. The lines shifted towards lower frequency are called Stokes lines, those shifted towards higher frequency are the anti-Stokes lines (see fig. 4).

It should be noted that nonrigid molecules also have vibrational transitions. These vibrational Raman lines, which are mostly very weak, appear at large distance from the exciting line and are not considered in this thesis.

2. *Scattered light intensities*. The amount of light scattered by dilute gases is usually extremely small and for most experimental studies the question of the scattered intensity is of great importance. A short discussion on this matter is therefore certainly appropriate.

Consider the scattering configuration of the preceding section (fig. 3). The incident light intensity per unit area is denoted by W_0, the scattering volume by V and the number density of the gas by n. It is assumed that the frequency changes involved in the scattering process are small so that for intensity calculations the scattered light frequency ν may be replaced by ν_0.

In this situation the total intensity of the depolarized component of the light scattered into a solid angle $d\Omega$ is given by:

$$I_{depol}\, d\Omega = W_0\, n\, V\, \frac{1}{15}\, (\alpha_{/\!/} - \alpha_{\perp})^2\, \left(\frac{2\pi\nu_0}{c}\right)^4\, d\Omega \quad , \tag{6}$$

with c the velocity of light in vacuum. For the polarized component one has

$$I_{pol}\, d\Omega = W_0\, n\, V\, \{\bar{\alpha}^2 + \frac{4}{45}\, (\alpha_{/\!/} - \alpha_{\perp})^2\}\, \left(\frac{2\pi\nu_0}{c}\right)^4\, d\Omega \quad . \tag{7}$$

Usually I_{depol} is much smaller than I_{pol}, which is due to the fact that the term with $\bar{\alpha}^2$, representing the Rayleigh-Brillouin triplet is by far the largest. The ratio I_{depol}/I_{pol}, denoted by D_0 is known as the depolarization ratio:

$$D_0 = \frac{3(\alpha_{/\!/} - \alpha_\perp)^2}{45\,\bar{\alpha}^2 + 4(\alpha_{/\!/} - \alpha_\perp)^2} \quad . \tag{8}$$

For most simple gases D_0 is of the order of 10^{-2} (see ref. 4).

The distribution of the intensity in the depolarized spectrum, *i.e.*, over the depolarized Rayleigh line and the rotational Raman lines, is easily calculated from the fractional populations of the rotational states p_j and the line strength factors (transition matrix elements) as given by Placzek and Teller[5]. The intensity of the depolarized Rayleigh line is given by

$$I_{DPR}\, d\Omega = W_0\, n\, V\, \frac{(\alpha_{/\!/} - \alpha_\perp)^2}{15} \left(\frac{2\pi\nu_0}{c}\right)^4 \sum_j p_j \frac{j\,(j+1)}{(2j-1)(2j+3)}\, d\Omega \quad . \tag{9}$$

The intensities of the rotational Raman lines are, for the Stokes transition $j \to j + 2$, given by

$$I_{RR}(j)\, d\Omega = W_0\, n\, V\, \frac{(\alpha_{/\!/} - \alpha_\perp)^2}{15} \left(\frac{2\pi\nu_0}{c}\right)^4 p_j \frac{3(j+1)(j+2)}{2(2j+1)(2j+3)}\, d\Omega. \tag{10}$$

For the anti-Stokes transition one has

$$I_{RR}(j)\, d\Omega = W_0\, n\, V\, \frac{(\alpha_{/\!/} - \alpha_\perp)^2}{15} \left(\frac{2\pi\nu_0}{c}\right)^4 p_j \frac{3(j-1)\,j}{2(2j-1)(2j+1)}\, d\Omega. \tag{11}$$

In the classical limit (high j) this leads to a situation in which $\frac{1}{4}$ of the depolarized intensity lies in the depolarized Rayleigh line and $\frac{3}{4}$ in the rotational Raman lines. It is easily verified that at room temperature the deviations from this classical limit are very small for most gases. In fact a significantly different intensity ratio is found only for the hydrogen isotopes.

To give an indication of the magnitude of the scattered intensity, $I_{DPR}\, d\Omega$ is calculated for N_2 at 1 atm and 293 K: n is about $2{\cdot}5 \times 10^{19}$ molecules/cm^3 and $\alpha_{/\!/} - \alpha_\perp$ has for N_2 the value $0{\cdot}7 \times 10^{-24}$ cm^3. A

100 mW He-Ne laser (λ = 6328 Å) is taken as a light source. The light scattered by the laser beam over a certain length, say 0.5 mm, is collected. (This defines the scattering volume V). The collecting angle is chosen as 10°. In this situation one finds for the intensity in the depolarized Rayleigh line a value of about $2{\cdot}5 \times 10^{-12}$ mW, which corresponds to some 8000 photons per second. In the experiment, the effectively measured intensity is even far less, mostly 50-100 photons per second. This is due to the fact that the efficiency of a typical detector is only a few percent and to various losses in the optical system.

3. Effects of collisions on the spectral lines. As pointed out before, the various components of the scattered light arise from density and anisotropy fluctuations in the gas. The corresponding line profiles are determined by the time evolution of these fluctuations[1]. In rarefied gases, *i.e.*, when the mean free path $\bar{\ell}$ of the molecules is large compared to λ, this time evolution is governed by the free translational motion of the molecules. For all components of the scattered light this results in the well-known Doppler profile, reflecting the velocity distribution of the individual molecules.

At higher densities, however, where $\bar{\ell} \ll \lambda$, collisional effects are important and the line profiles are modified. The molecular motions can no longer be considered as uncorrelated and therefore the scalar scattering, which arises from fluctuations of the density, reflects the interference between light scattered from different molecules at different times. The triplet structure of the scattered light (Rayleigh-Brillouin triplet) is thus, in fact, of a bulk nature.

On the other hand, the scattering due to fluctuations in the molecular orientations, *i.e.*, the depolarized Rayleigh and rotational Raman scattering, may still be looked upon as arising from independent scatterers since in dilute gases there is no correlation in orientarion or rotational motion of different molecules. The spectral profiles reflect therefore the time evolution of the internal states of the individual molecules under the influence of collisions. This process gives rise to a broadening of the lines, which, in the binary collision regime, is linear with density. It is this pressure or collisional broadening

that is the subject of this thesis. The broadening processes are now considered in more detail.

As indicated above, the pressure broadening of the depolarized Rayleigh and rotational Raman lines arises because collisions tend to disturb the internal states of the radiating molecules. The disturbance can be brought about in three different ways[6]:

a) Complete interruption of the radiation process due to collisional changes of j (energetically inelastic collisions).
b) Amplitude modulation of the scattered radiation by collisional reorientation of the radiating dipole.
c) Rotational phase shifts by elastic collisions.

For a discussion of depolarized Rayleigh scattering the (rotating) molecules may be considered as discs of which only the orientation in space is important and not the rotational motion as such. As a consequence, the broadening of the depolarized Rayleigh line is insensitive to collisional changes of j or to rotational phase shifts. Only collisional reorientation leads to line broadening. The broadening rate is a measure for the efficiency of this process.

In the broadening of rotational Raman lines, on the other hand, all three broadening mechanisms play a role, but the phase shift contribution is usually very small. An important aspect is here that from an investigation of the broadening for a series of Raman lines information can be obtained about the dependence of collision processes on the rotational states of the molecules.

The direct information on collision processes between nonspherical molecules, obtained from pressure broadening studies, is very valuable as it leads to a better knowledge of the angle-dependent part of the intermolecular potential.

4. Survey of the experiments. In this thesis results are presented of a study of the pressure broadening of the depolarized Rayleigh line and the rotational Raman lines of various gases at room temperature. In chapter I a description is given of the experimental setup used for the light scattering studies. The broadening of the depolarized Rayleigh line is investigated for the gases normal H_2, para H_2, HD, normal D_2, N_2,

CO, CO_2 and OCS. It is shown that the line shape associated with the broadening of the depolarized Rayleigh line deviates in general from the Lorentzian profile that was found in earlier investigations. This result is attributed to a dependence of the molecular reorientation probability on the rotational state (gyroscopic stability). The results of the depolarized Rayleigh experiments appear to be extremely useful for testing general kinetic theories which have been used for the description of phenomena such as, *e.g.*, the Senftleben-Beenakker effect for the viscosity and nuclear magnetic relaxation.

In Chapter II the depolarized Rayleigh experiments are extended to the broadening of the depolarized Rayleigh line by noble gases. Such experiments are desirable since the interaction between a spherical and a nonspherical particle is more simply described than the interaction between two nonspherical particles. Results are presented regarding the broadening of the depolarized Rayleigh line in N_2 by the noble gases He, Ne and Ar.

In chapter III results are given of experiments on the collisional broadening of the rotational Raman lines in the hydrogen isotopes. The broadening of the Raman lines has been investigated as a function of rotational quantum number j and, for H_2, also as a function of ortho-para composition. Conclusive evidence is obtained for the occurrence of so-called resonance collisions. These are collisions in which the rotational energy given up by one molecule is exactly matched by the rotational energy picked up by its collision partner. The observed behavior is compared with that predicted by theory[7].

References.

1. Landau, L.D. and Lifshitz, E.M., Electrodynamics of Continuous Media (Pergamon Press, Oxford, 1960).
2. Hess, S., Z. Naturforsch. *24a* (1969) 1675; *25a* (1970) 350.
3. Hess, S., Springer Tracts Mod. Phys. *54* (1970) 136.
4. Bridge, N.J. and Buckingham, A.D., Proc. Roy. Soc. (London) Ser. *A 295* (1966) 334.
5. Placzek, G. and Teller, E., Z. Physik *81* (1933) 209.
6. Gordon, R.G., J. Chem. Phys. *44* (1966) 3083.
7. Van Kranendonk, J., Can. J. Phys. *41* (1963) 433.

CHAPTER I

THE PRESSURE BROADENING OF THE DEPOLARIZED RAYLEIGH LINE: PURE GASES OF LINEAR MOLECULES

1. Introduction. It has long been known that the study of pressure broadening of spectral lines in gases of polyatomic molecules provides information on molecular collisions and intermolecular forces[1]. The particular significance, however, of the study of the broadening of the depolarized Rayleigh line in the light scattering spectrum of linear molecules was first discussed by Gordon in 1966[2]. The frequency distribution of this line is determined by the lifetime of orientational fluctuations in the gas and is therefore a measure for the ability of collisions to reorient the rotational angular momentum $\underline{J}$. This can be illustrated by the following simple picture. The incoming polarized light induces a high frequency electric dipole in a molecule. Because of the anisotropy of the molecular polarizability this dipole is not necessarily parallel to the exciting field (see also the introduction to this thesis). Therefore the scattered light contains a component with polarization perpendicular to that of the exciting radiation. Collisional reorientation of the molecule leads to an amplitude modulation of the effective radiating dipole and thus gives rise to broadening of the line. Since molecular reorientation is directly related to the angle-dependent part of the intermolecular potential, very specific information on this part of the potential can be obtained from a study of the pressure broadening of the depolarized Rayleigh line.

The first experimental study on depolarized Rayleigh light scattering was reported by Cooper *et al.*[3], who investigated the depolarized Rayleigh line for the gases H_2, N_2 and CO_2 at roomtemperature. They reported that the line shape was Lorentzian and observed a broadening linear with density. In two subsequent studies on depolarized Rayleigh scattering[4,5] similar results were obtained.

In this study, however, it is shown from a careful analysis of new experimental data on a large number of molecules, that significant deviations from a Lorentzian profile do occur. Such deviations point

to the fact that a one-decay-time description is not applicable. Indications of similar deviations have also been observed in another phenomenon governed by collisional reorientation, namely, the Senftleben-Beenakker effect for the viscosity[6-8]. Whereas in those experiments the situation is too complicated to obtain quantitative information from the occurrence of such deviations, the study of the pressure broadening of the depolarized Rayleigh line is very well suited for this purpose. Furthermore, it allows a critical evaluation of kinetic theories for relaxation and transport phenomena in gases of linear molecules.

Preliminary results of this study have been presented earlier[9]. In this chapter we will present results regarding the broadening of the depolarized Rayleigh line for the gases normal H_2, para H_2, HD, normal D_2, N_2, CO, CO_2 and OCS, all at room temperature. Results on mixtures of N_2 with the noble gases He, Ne and Ar will be given in chapter II. The observed behavior is used to test various theoretical descriptions of depolarized Rayleigh line broadening. Finally the results are expressed as effective cross sections and compared with related cross sections obtained from experiments on nuclear magnetic relaxation and on the Senftleben-Beenakker effect for the viscosity.

2. *Experimental.* 2.1 General. A schematic diagram of the experimental setup is shown in fig. 1. The beam from a He-Ne laser operating at 6328 Å was focussed into a pressure cell containing the gas under study. The polarization direction of the laser light was vertical to the scattering plane. Light scattered at 90° to the incident beam was collected and passed through a Glan-Thompson prism to eliminate the strong vertically polarized isotropic component. The Rayleigh line was isolated in the depolarized spectrum by means of a narrow band interference filter. For the spectral analysis a pressure scanned Fabry-Pérot interferometer was used. The detection system consisted of a cooled photomultiplier in combination with standard photon counting equipment.

We now discuss some aspects of the experimental setup in more detail.

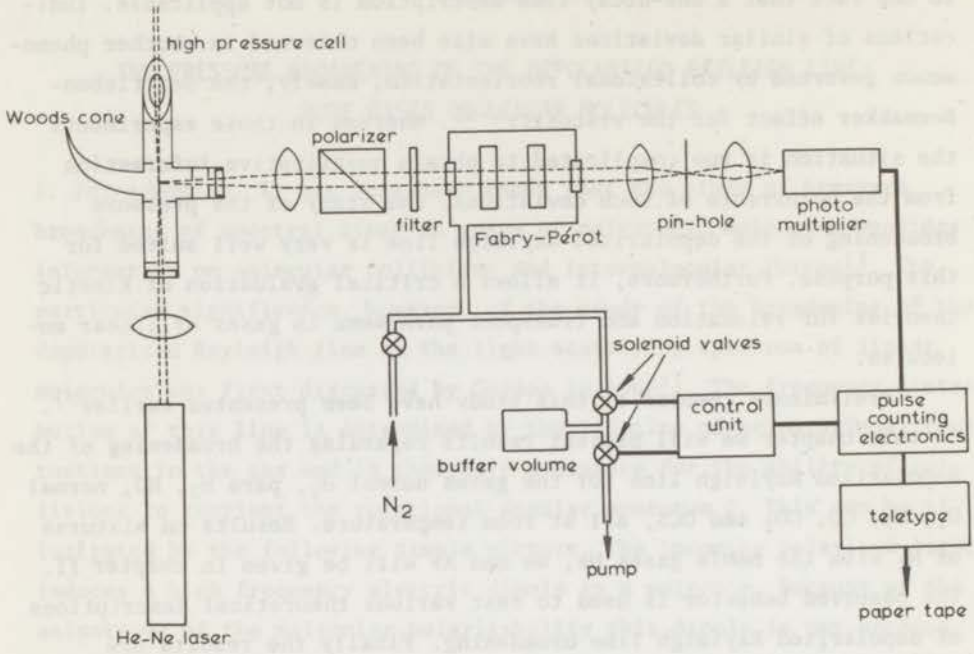

Fig. 1. Schematic diagram of the experimental setup.

2.2 Laser. The laser was a Spectra Physics model 125 A He-Ne laser giving about 70 mW power at 6328 Å. This power level was monitored during the experiment and variations over one experimental run were always less than 1%. The laser line profile contributed to the overall instrumental width (see section 2.6); the individual laser modes were not resolved in these experiments.

2.3 Pressure cell. Special attention was paid to the design of the high pressure scattering cell to minimize the amount of direct laser light that reaches the detector via internal reflections in the cell. After several improvements the best results were finally obtained with the cell shown schematically in fig. 1. The entrance and exit windows for the laser beam were made out of fused silica and located as far from the center of the cell as convenient. The exit window was positioned at the Brewster angle. Anti-reflection coatings were not used on these windows since they cause a drastic increase of scattered laser

light from the window surfaces. A Wood's cone of black glass provided a dark background for the detector. The inner part of the cell was made flat black and a special arrangement of diaphragms was positioned inside as indicated in fig. 1.

For the viewing window no fused silica was used since in combination with standard rubber "O" ring sealings it gives rise to a relatively high and strongly pressure dependent depolarization of light. Therefore this window was made out of "zero stress optical coefficient" glass (Chance-Pilkington, Great Britain), of the type used as window material in Kerr cells[10]. With this special glass no depolarization effect was observed up to pressures of 100 atm. Anti-reflection coatings were used because of the high index of refraction of this material.

For alignment purposes the cell was provided with a screen that could be lowered into the laser beam at the point of focus.

2.4 Polarizing prism. Since the polarized scattered light was usually a factor 100-1000 more intense than the depolarized Rayleigh signal a very efficient suppression of the polarized component was necessary. The Glan-Thompson polarizing prism that was used had a rejection ratio of about 10^{-5}. The effective rejection ratio, however, was poorer due to a depolarization of light in between the scattering area and the polarizing prism and also due to the focussing of the laser beam and the finite viewing angle of about 10°. Using zero-stress glass for the viewing window and the collecting lens an effective rejection ratio of 1.5×10^{-5} was obtained. This is about an order of magnitude better than previously obtained in this type of experiment.

2.5 Interference filter. For an investigation of the spectral line profile with a Fabry-Pérot interferometer, it is desirable to isolate the depolarized Rayleigh line from the rotational Raman lines, which also occur in the depolarized spectrum (see fig. 4 of the general introduction). For the diatomic molecules H_2, HD, D_2, N_2 and CO a narrowband interference filter centered at 6328 Å was used. The bandwidth of this filter was about 8 Å *. For the hydrogen isotopes this was sufficient to suppress all Raman scattered light. For the gases N_2 and CO,

* By bandwidth the full width at half height is meant; half-width is always used when referring to half the width at half height.

however, a fraction of the first rotational Raman line on either side of the Rayleigh line was transmitted.

For the molecules CO_2 and OCS the separation between the various lines is so small that the 8 Å filter would transmit a relatively large fraction of the Raman intensity. In these cases no filter was used so that the Raman lines contributed freely to the observed spectrum. The way in which we corrected for the Raman contributions will be discussed in section 3.

2.6 Interferometer system. For the high resolution spectral analysis required in these experiments, a Fabry-Pérot interferometer system was used. The Fabry-Pérot etalon consisted of two flat mirrors (Perkin and Elmer), polished to $\lambda/100$ and coated for 95% reflection at 6328 Å. The mirrors were contained in a solid mount and separated by an invar spacer. In the experiments two spacers were used with thickness of 0.175 cm and 0.379 cm. The light transmitted by the etalon was focussed onto a small pinhole thus selecting out the zero-order fringe of the Fabry-Pérot ring pattern. The etalon mount was placed in an aluminum chamber filled with N_2 at about 1 atm. Scanning of the spectrum was performed by varying the N_2 pressure in that chamber thus changing the index of refraction (n_r) between the etalon mirrors. It was found convenient to vary the pressure in steps. At a constant pressure in the interferometer chamber photons were counted during a fixed time interval. After completion of this counting interval the pressure was lowered by letting out an amount of gas into a buffer volume. Then the next counting cycle was started and the buffer volume was evacuated again. Constant pressure steps were obtained automatically by using a pressure switch (in the buffer volume) in combination with two solenoid valves (see fig. 1).

A few examples of experimentally recorded spectra (interferograms) are shown in fig. 2. The number of steps (or spectral points) was typically 400. The two peaks correspond to two consecutive transmission orders of the interferometer. The frequency interval corresponding to the distance between these peaks is known as the free spectral range (FSR). One has the relation $FSR = c/2n_r d$, d being the mirror spacing and c the velocity of light in vacuum. FSR serves as a frequency refer-

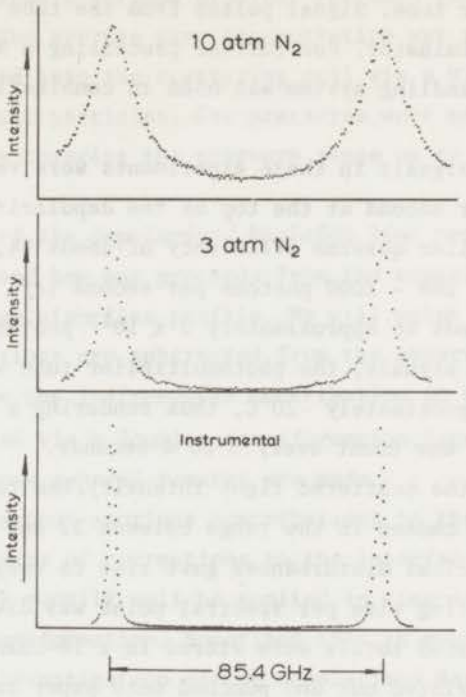

Fig. 2. Interferograms of the depolarized Rayleigh line in N_2 at 10 atm. and 3 atm. The two peaks correspond to two consecutive orders of the Fabry-Pérot interferometer. The bottom curve shows the unbroadened instrumental profile.

ence for the analysis of the interferograms. In the experiments FSR had the values 39.5 GHz and 85.4 GHz.

Fig. 2 also gives an example of an instrumental profile, *i.e.*, the unbroadened laser line as transmitted by the interferometer. To obtain such a profile the screen in the scattering chamber was lowered into the laser beam giving a large amount of diffuse laser light in the scattering direction. Over a set of experiments the instrumental profile remained always constant. The overall finesse, *i.e.*, the ratio of free spectral range and instrumental bandwidth, was about 25 for FSR = 39.5 GHz and 33 for FSR = 85.4 GHz. The difference is due to the unequal relative contributions of the laser linewidth in the two cases.

2.7 Detection system. After having passed the interferometer system the light was focussed onto the S 20 photocathode of an ITT FW

130 photomultiplier tube. Signal pulses from the tube were amplified and passed a discriminator. For further processing a Nuclear Data series 1100 data-handling system was used in combination with a ND 536 CTB time base.

The detected signals in these experiments were very low, typically 10 - 100 counts per second at the top of the depolarized Rayleigh line. With a photomultiplier quantum efficiency of about 5%, this corresponds to an intensity of 200 - 2000 photons per second (*cf*: the 70 mW laser intensity corresponds to approximately 2×10^{17} photons per second). Because of the low signals, the photomultiplier tube was cooled thermoelectrically to approximately -20°C, thus rendering a sufficiently low darkcount level of one count every 3 to 4 seconds.

Depending on the scattered light intensity, the counting time per spectral point was chosen in the range between 32 and 160 seconds. Occasionally electrical disturbances gave rise to very high counts. Therefore the counting time per spectral point was divided into 16 equal parts. The accumulated totals were stored in a 16-channel digital memory and subsequently printed out and punched onto paper tape via an ITT Teletype. Spurious high counts could easily be rejected in the computer analysis of the data. The duration of a typical scan varied from 2-20 hours.

2.8 Gas handling. The gases H_2, D_2, CO, N_2, CO_2 and OCS were obtained commercially and had a purity of better than 99%, with the exception of OCS, which had a purity of 97% with as main contamination CO_2. HD was prepared by the action of $LiAlH_4$ on D_2O following a method described by Fookson *et al.*[11]. After removal of small amounts of H_2 and D_2 by fractional distillation, a purity of better than 99% was obtained.

For H_2, experiments were performed on normal H_2 (nH_2), *i.e.*, 3/4 ortho (odd rotational states) and 1/4 para (even rotational states) and on para H_2 (pH_2). For D_2 only the normal composition (nD_2) was studied, *i.e.*, 2/3 ortho (even states) and 1/3 para (odd states).

Para H_2 was prepared by condensing normal H_2 on a catalyst at 20 K. During the light scattering experiment pH_2 slowly converted back to nH_2. Over one experimental run the concentration change was only a few per-

cent and did not form a serious problem. For each run a fresh sample of pH_2 was used. The average para concentration was about 95%.

Gases were led into the scattering cell via a Millipore filter in order to remove dust particles. Gas pressures were measured with two Bourdon manometers covering the pressure range up to 150 atm.

3. Determination of the depolarized Rayleigh line profile. In this section it is discussed how one proceeds from the experimental data to the net depolarized Rayleigh line profile. We will point out how several unwanted contributions are subtracted from the observed spectra. It is then discussed how the instrumental contribution to the spectral profile can be removed via a Fourier transformation into time domain. First, however, some general remarks are made.

a) Although the various spurious contributions to the spectra are discussed in terms of corrections to the interferograms, these corrections may equally well be applied in time domain, *i.e.*, after the Fourier transformation. Sometimes this is even more convenient.
b) For a careful investigation of the depolarized Rayleigh line profile and a determination of possible deviations from a Lorentzian shape the most critical corrections are those that are peaked functions of the frequency (see, *e.g.*, 3.2 and 3.3), since they easily distort the actual line shape. Most of the other contributions that have to be removed from the observed spectra appear as a flat background in the interferograms. The final conclusion on whether or not the depolarized Rayleigh line profile deviates from a Lorentzian shape is not very sensitive to such contributions.
c) A reliable indirect test on whether the corrections are carried out correctly is provided by the scaling procedure in time domain, that is applied to the final results (see section 4.1).

3.1 Photomultiplier darkcount. The photomultiplier darkcount level was measured several times during a set of experiments. It was very stable (typically 0.3 counts per second) and subtracted from the observed spectrum as a constant level.

3.2 Vacuum stray light. Some parasitic laser light reached the detector via internal reflections in the cell. This contribution could

be determined by measuring the signal from the evacuated cell. The line shape of this signal was identical to that of the instrumental profile. Its peak intensity was measured between experimental runs. In the early stage of the experiments an intensity correction of the order of 0.4 counts per second (peak value) had to be applied. With the final version of the scattering cell no correction was necessary.

3.3 Polarized stray light. The very intense polarized component of the scattered light (Rayleigh-Brillouin triplet) could not be suppressed completely in the experiments. The (small) fraction of this light reaching the detector is referred to as polarized stray light. To be able to subtract this contribution from the observed interferograms one needs to know its shape and (relative) intensity. The spectral shape for the various gases was determined by scanning the polarized light after rotating the polarizer over 90°. The ratio of polarized stray intensity to depolarized Rayleigh intensity is for each gas, independent of the density, given by the factor* $60\ R\ \bar{\alpha}^2/(\alpha_{/\!/} - \alpha_\perp)^2$, where R is the effective rejection ratio of the system. $\alpha_{/\!/}$ and $\alpha_\perp$ are the molecular polarizabilities in directions along the internuclear axis and perpendicular to it, respectively. $\bar{\alpha}$ is the average polarizability, given by $\bar{\alpha} = 1/3\ (2\alpha_\perp + \alpha_{/\!/})$.

This ratio was experimentally determined for one gas, *e.g.* CO, by measuring the spectrum at high density, where the narrow polarized stray peak appears as a well resolved line on top of a very broad depolarized Rayleigh line (see fig. 3). Using the value for $(\alpha_{/\!/} - \alpha_\perp)/\bar{\alpha}$ of CO as determined in depolarization studies (see table I), the rejection ratio R can be determined and is found to be about 1.5×10^{-5}. The intensity corrections for the other gases can then be obtained using the values of $(\alpha_{/\!/} - \alpha_\perp)/\bar{\alpha}$ for these gases as given in table I. The polarized stray intensities thus obtained are also given.

As a check, the effective rejection ratio R was also determined by

* We have used here that 1/4 of the depolarized intensity lies in the depolarized Rayleigh line. For the hydrogen isotopes, where only a few rotational levels are occupied, this is not correct. The proper factor in that case was obtained by using the intensity expressions given in the introduction to this thesis. See also the discussion on this subject in ref. 12.

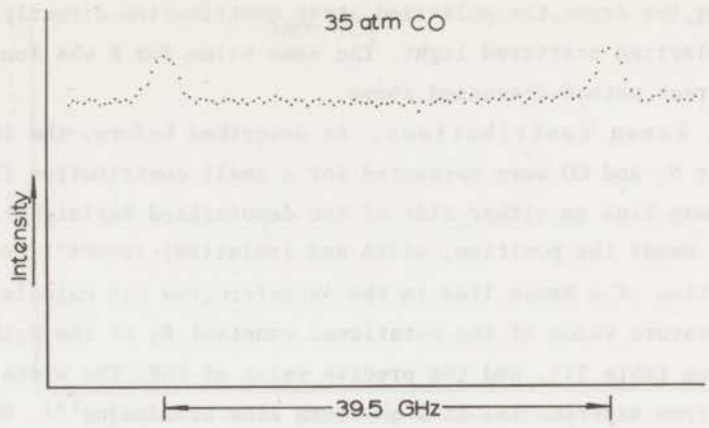

Fig. 3. Determination of the amount of polarized light in the interferograms at high density. The small peaks represent the polarized stray contribution; the depolarized Rayleigh line gives rise to an almost flat background.

Table I

Polarizability data and polarized stray correction

	$\bar{\alpha}$ ($Å^3$)		$\frac{\alpha_{/\!/} - \alpha_{\perp}}{\bar{\alpha}}$		$\frac{\text{pol. stray int.}}{\text{dep. Rayleigh int.}} \times 10^2$
nH_2	0.82	a)	.38[5]	c)	0.5
pH_2	0.82	b)	.38[5]	d)	1.2
HD	0.82	b)	.38	d)	0.6
nD_2	0.81	a, b)	.37	c)	0.7
N_2	1.76	a)	.39	c)	0.6
CO	1.99	a)	.27	c)	1.3
CO_2	2.65	a)	.80	c)	0.1[5]
OCS	5.24	a)	.90	e)	0.1

a) ref. 13
b) ref. 14
c) ref. 12
d) estimated value, see ref. 15
e) ref. 16

comparing, for Argon, the polarized stray contribution directly with the total polarized scattered light. The same value for R was found as in the indirect method discussed above.

3.4 Raman contributions. As described before, the interferograms for N_2 and CO were corrected for a small contribution from the first Raman line on either side of the depolarized Rayleigh line. For this one needs the position, width and (relative) intensity of these lines. The position of a Raman line in the interferogram was calculated from the literature value of the rotational constant B_0 of the molecule under study (see table II), and the precise value of FSR. The width was estimated from experimental data on Raman line broadening[19]. The intensity of the Raman line relative to the depolarized Rayleigh intensity was

Table II

Values of the rotational constant B_0

	B_0 (cm^{-1})	reference
N_2	1.98951	17
CO	1.92252	18
CO_2	0.39021	21
OCS	0.20286	22

calculated from the populations of the rotational states and the line strength factors for Raman scattering as given by Placzek and Teller[20] (see the expressions in the introduction to this thesis). The magnitude of the correction was then obtained using the transmission curve of the 8 Å filter. For N_2 the intensity correction was about 5% of the total intensity, for CO 4%.

In the experiments on CO_2 and OCS all rotational Raman lines contributed freely to the observed spectra, as no filter was used. For these molecules, however, the large number of Raman lines only gave rise to an unresolved background in the interferograms (see fig. 4). Using the values for FSR, the rotational constant B_0 (see table II),

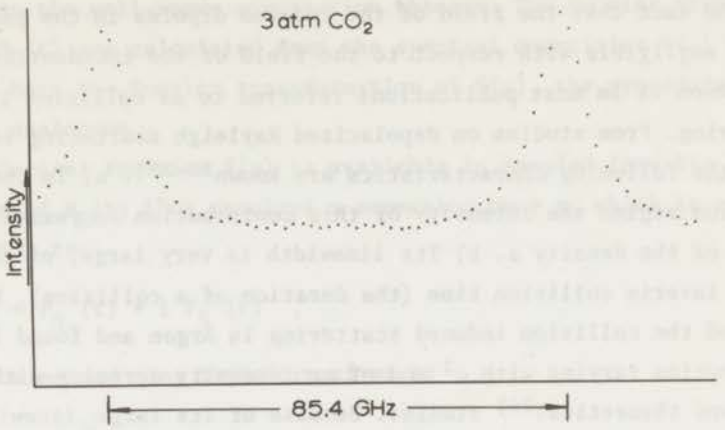

Fig. 4. Interferogram for CO_2. The depolarized Rayleigh line appears on top of an unresolved Raman continuum.

the Raman line broadening coefficients* and the intensities of the various lines, the intensity distribution of these Raman lines over the interferogram could be calculated. As a result of this calculation a completely flat Raman continuum was found, with only in one case (CO_2, FSR = 85.4 GHz) a slight modulation. The Raman background could then be subtracted from the experimental interferograms by making use of the fact that the summed intensity of the Raman lines is $\frac{3}{4}$ of the total depolarized intensity.

3.5 Wing correction. In a few cases the depolarized Rayleigh line was so wide that a small amount of the intensity in the far wings was not transmitted by the interference filter. In the interferograms this results effectively in a flat background contribution with negative intensity. A correction for this effect, which is only significant for a few gases at the highest pressures and never amounts to more than 3% of the total intensity, has been applied.

3.6 Collision induced scattering. At high densities an additional contribution to the spectrum becomes important, which arises

* CO_2 broadening coefficients have been obtained from ref. 19. For OCS no data were available, but the broadening coefficients will certainly be larger than for CO_2. Performing the calculations for OCS with the CO_2 broadening coefficients led to the flat background result mentioned in the text.

from the fact that the field of the induced dipoles in the gas is no longer negligible with respect to the field of the incident light. This phenomenon is in most publications referred to as collision induced scattering. From studies on depolarized Rayleigh scattering in noble gases the following characteristics are known[23-25]: a) In the binary collision regime the intensity of this contribution increases with the square of the density ρ. b) Its linewidth is very large, of the order of the inverse collision time (the duration of a collision). We have measured the collision induced scattering in Argon and found indeed a contribution varying with ρ^2 and of an intensity agreeing with experimental[23] and theoretical[26] studies. Because of its large linewidth the collision induced line appears in the interferograms as a flat background.

Recently a theoretical expression for the collision induced intensity for linear molecules has been given[27]. Using this theoretical formula, we corrected our results for collision induced scattering. The fact that the collision induced line is only partly transmitted by the 8 Å interference filter was taken into account. Its effective intensity as a fraction of the total depolarized Rayleigh intensity was found to be at the most about 2% at the highest pressures investigated. The contribution was subtracted from the interferograms as a flat background.

3.7 Fourier transformation. At this stage, after having removed the various parasitic contributions, the interferogram, described by a function $S(\nu)$, is a convolution of the true depolarized Rayleigh line $R(\nu)$ with the periodic instrumental function $O(\nu)$:

$$S(\nu) = R(\nu) * O(\nu) = \int_{-\infty}^{+\infty} R(\nu') O(\nu - \nu')\, d\nu' . \qquad (1)$$

The problem in the analysis is to obtain $R(\nu)$ from the experimental quantities $S(\nu)$ and $O(\nu)$. This deconvolution problem is most easily solved by a Fourier transformation into time domain[28]. The relationship between the Fourier transforms of the functions in eq. (1) is given by a simple product:

$$F_S(t) = F_R(t) \cdot F_O(t) , \qquad (2)$$

according to the well-known convolution theorem. The Fourier transforms $F_S(t)$ and $F_O(t)$ are calculated from the spectral quantities $S(\nu)$ and $O(\nu)$. We discuss here the Fourier transformation of $S(\nu)$, the procedure for $O(\nu)$ being analogous.

The spectral function $S(\nu)$ is available in sampled form $S(\nu_n)$. The calculation of $F_S(t)$ thus requires a summation over n, which is carried out according to:

$$F_S(t) = F_S^{+}(t) + i\, F_S^{-}(t) \quad , \tag{3}$$

with the cosine and sine transform given by

$$F_S^{+}(t) = \frac{\sum_{n=1}^{N} S(\nu_n) \cos 2\pi\, \nu_n t}{\sum_{n=1}^{N} S(\nu_n)} \tag{4}$$

and

$$F_S^{-}(t) = \frac{\sum_{n=1}^{N} S(\nu_n) \sin 2\pi\, \nu_n t}{\sum_{n=1}^{N} S(\nu_n)} \quad . \tag{5}$$

Because of the periodicity of $S(\nu)$ the summation over n can be confined to one free spectral range ($N \approx 250$) and is only carried out at discrete times $t = \ell T$ (with $\ell = 0, 1, 2 \ldots$ and $T = 1/FSR$). $F_S(t)$ will be identically zero for all intermediate t. As the frequency zero was assigned to the center of the peak, the sine transform (eq. (5)) is a measure for the line symmetry, In all cases we found this sine transform to be zero. As a consequence the Fourier transform $F_S(t)$ is given by the expression for the cosine transform (eq. (4)). The normalization has been chosen such that $F_S(0) = 1$. Examples of $F_S(t)$ and $F_O(t)$ are shown in fig. 5. $F_R(t)$, the Fourier transform of the depolarized Rayleigh line profile is now obtained as the ratio of $F_S(t)$ and $F_O(t)$.

Rather than transform back to frequency domain to obtain $R(\nu)$ it proves advantageous to interpret the results in time domain. This can be illustrated in the following way. Assume $R(\nu)$ has a Lorentzian form:

$$R(\nu) = \frac{I_0}{\pi} \; \frac{\Delta\nu_{\frac{1}{2}}}{\nu^2 + \Delta\nu_{\frac{1}{2}}^{\,2}} \, , \tag{6}$$

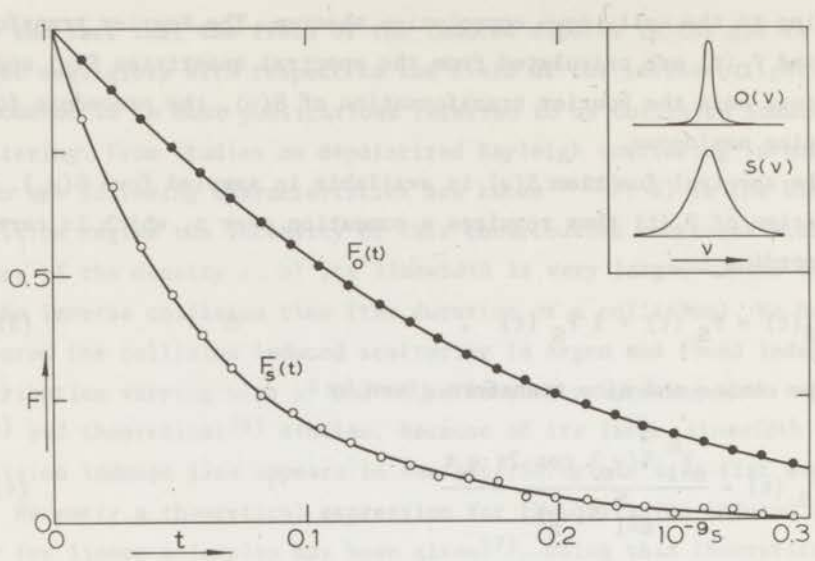

Fig. 5. Fourier transforms of the experimental interferograms.
$F_S(t)$: Fourier transform of the spectral profile S(ν) for N_2 at 3 atm.
$F_0(t)$: Fourier transform of the instrumental profile O(ν).

where $\Delta\nu_{\frac{1}{2}}$ is the half-width at half intensity and the central frequency has been taken zero. I_0 is the total integrated intensity of the line:

$$I_0 = \int_{-\infty}^{+\infty} R(\nu)\, d\nu \ .$$

For $F_R(t)$ one obtains now a simple exponential:

$$F_R(t) = e^{-2\pi\, \Delta\nu_{\frac{1}{2}}\, t} \ . \qquad (7)$$

Log $F_R(t)$ *versus* t obviously gives rise to a straight line and $\Delta\nu_{\frac{1}{2}}$ is then easily determined from the slope.

In a situation where deviations from the Lorentzian shape might occur the Fourier transformation is all the more useful since a plot of log $F_R(t)$ *versus* t provides a very sensitive test on the line shape. Even small deviations from the Lorentz shape would give a departure from a straight line.

4. Experimental results. 4.1 General. Results have been obtained for the depolarized Rayleigh line of the gases nH_2, pH_2, HD, nD_2, N_2, CO, CO_2 and OCS, all at 293 K. The experiments on the hydrogen isotopes were carried out in the pressure range from 20-110 atm. For the other gases pressures were in the range from 2-12 atm. For one gas (CO_2) also a series of experiments has been performed using an Argon ion laser operating at 5145 Å (see chapter III[29]). In this way it was verified that the pressure broadening is independent of the frequency of the incident light.

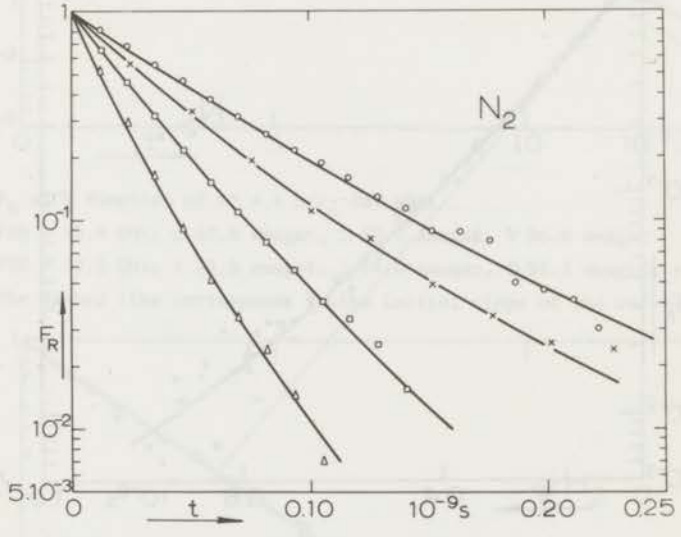

Fig. 6. Fourier transforms of the (net) depolarized Rayleigh line.
F_R as a function of time for N_2 at various densities.
FSR = 85.4 GHz; ○ 2.80 amagat, □ 5.60 amagat, Δ 9.39 amagat.
FSR = 39.5 GHz; x 3.73 amagat.
A density of 1 amagat corresponds approximately to 2.687 10^{19} molecules/cm^3.

A typical result is shown in fig. 6 giving F_R *versus* t for N_2 at various densities in a semilogarithmic plot. Deviations from linear behavior occur at all densities. A check on these results is provided by the fact that the depolarized Rayleigh line should broaden linearly

with the density ρ. In time domain this leads to the introduction of a reduced time scale.

$$t^* = t\,\rho/\rho_0\ , \tag{8}$$

with ρ_0 the density at s.t.p. (= 1 amagat). It is indeed found that all experimental points for N_2, corresponding to different densities, can be brought together onto one curve by plotting F_R *versus* t^* (see fig. 7).

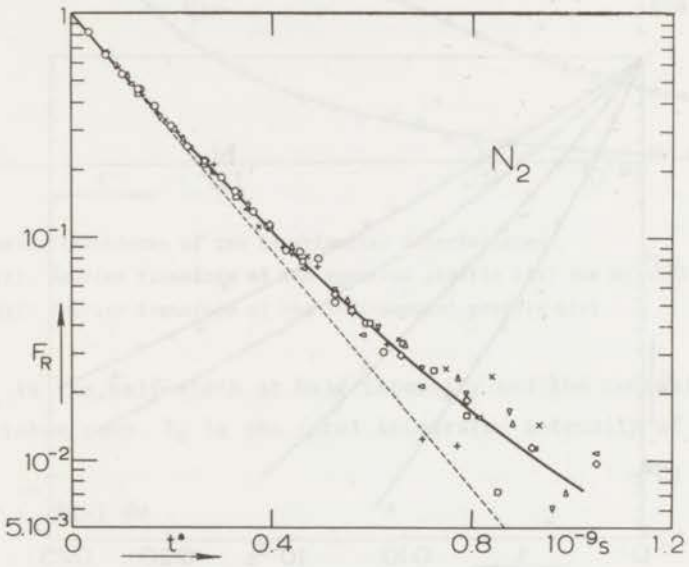

Fig. 7 F_R as a function of $t^* = t\,\rho/\rho_0$ for N_2.
FSR = 85.4 GHz; ○ 2.80 amagat, □ 5.59 amagat, ▽ 7.46 amagat,
△ 9.39 amagat, ◇ 11.21 amagat.
FSR = 39.5 GHz; + 2.80 amagat, X 3.73 amagat, ◁ 4.66 amagat.
The dashed line corresponds to the initial slope of the curve.

A similar procedure was followed for the other gases investigated and the results are presented in figs. 8-14.

A careful inspection of the graphs reveals that for all gases F_R is a unique function of t^*. The scatter in the experimental points is completely random and shows no correlation with the gas density. This implies that the broadening of the depolarized Rayleigh line is indeed

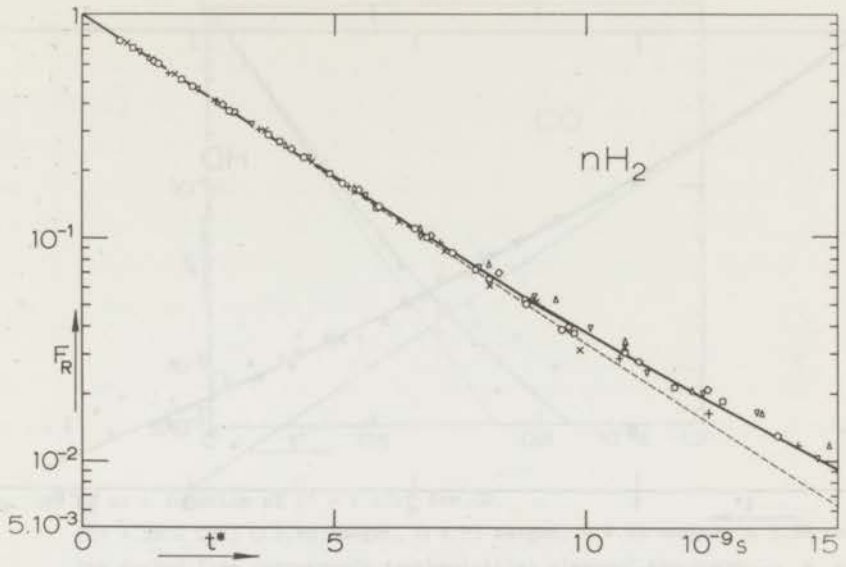

Fig. 8. F_R as a function of $t^* = t\ \rho/\rho_0$ for nH_2.
FSR = 85.4 GHz; ○ 62.8 amagat, □ 83.7 amagat, ▽ 96.0 amagat.
FSR = 39.5 GHz; X 35.5 amagat, △ 54.0 amagat, ◇ 55.3 amagat, + 71.1 amagat.
The dashed line corresponds to the initial slope of the curve.

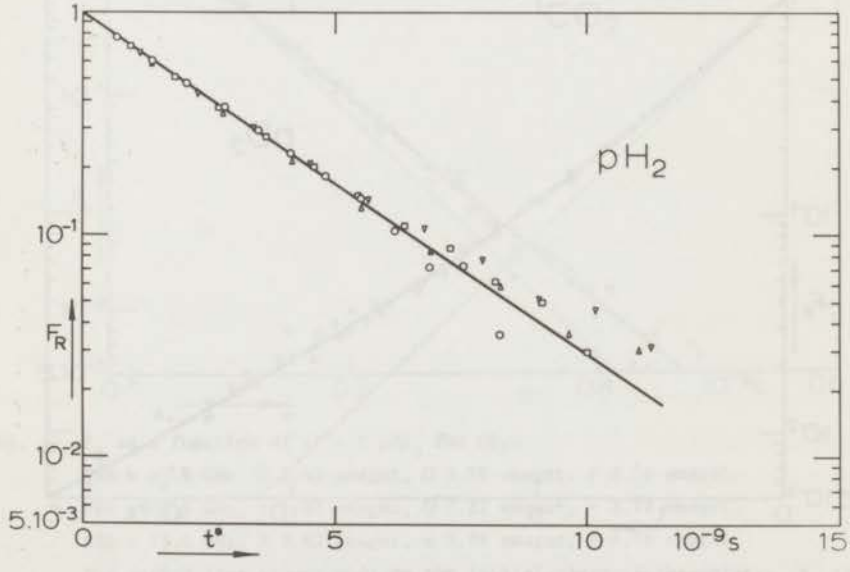

Fig. 9. F_R as a function of $t^* = t\ \rho/\rho_0$ for pH_2.
FSR = 39.5 GHz; ○ 27.5 amagat, □ 36.4 amagat, ▽ 45.3 amagat, △ 55.3 amagat.

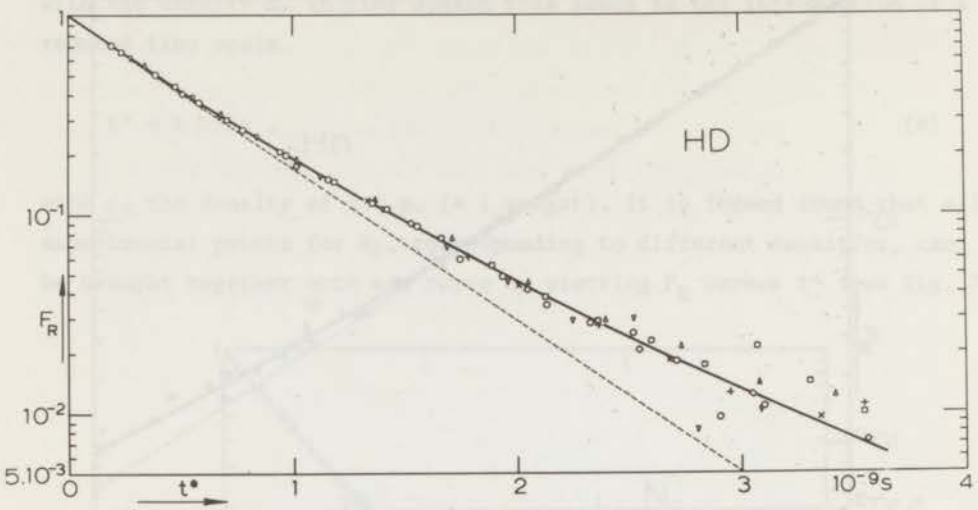

Fig. 10. F_R as a function of $t^* = t\,\rho/\rho_o$ for HD.
FSR = 85.4 GHz; ○ 16.6 amagat, □ 20.2 amagat, ▽ 24.0 amagat, △ 29.3 amagat,
◇ 43.5 amagat, + 50.5 amagat, X 57.3 amagat.
The dashed line corresponds to the initial slope of the curve.

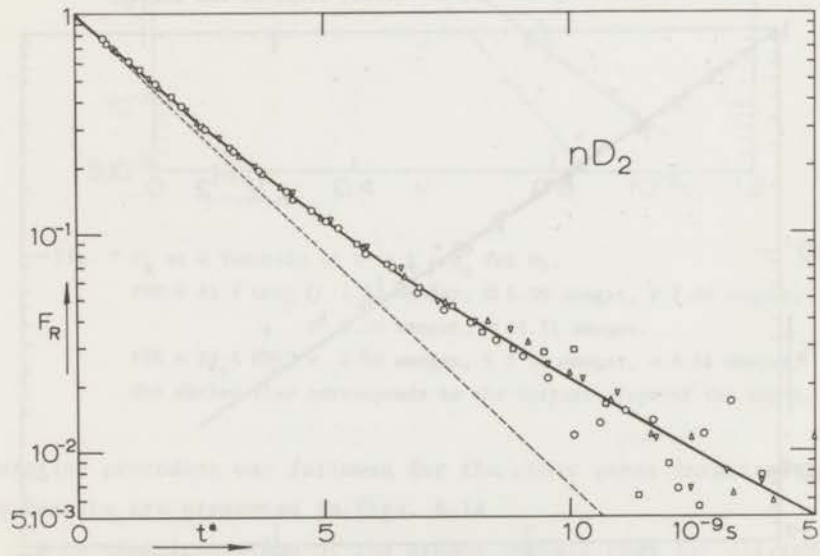

Fig. 11. F_R as a function of $t^* = t\,\rho/\rho_o$ for nD_2.
FSR = 85.4 GHz; ○ 45.4 amagat, □ 54.0 amagat, ▽ 62.8 amagat, △ 71.1 amagat.
The dashed line corresponds to the initial slope of the curve.

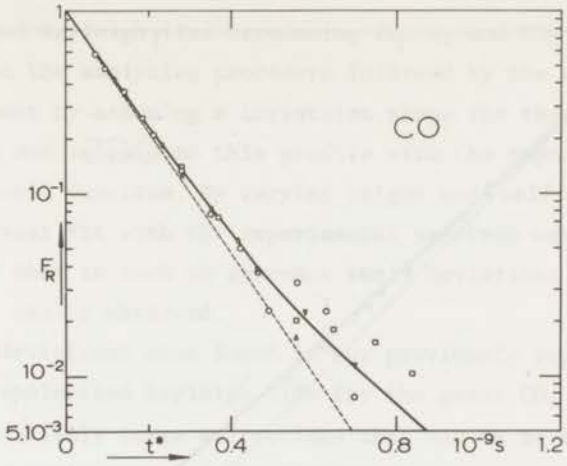

Fig. 12. F_R as a function of $t^* = t\ \rho/\rho_o$ for CO.
FSR = 39.5 GHz; ○ 2.80 amagat, □ 3.73 amagat, ▽ 4.66 amagat, △ 5.59 amagat.
The dashed line corresponds to the initial slope of the curve.

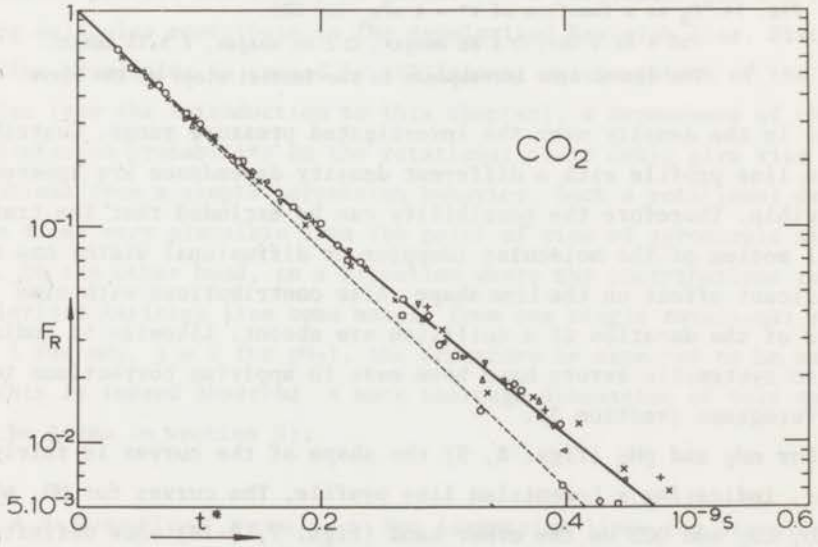

Fig. 13. F_R as a function of $t^* = t\ \rho/\rho_o$ for CO_2.
FSR = 85.4 GHz; ○ 2.82 amagat, □ 3.78 amagat, ▽ 4.76 amagat.
FSR = 39.5 GHz; △ 1.87 amagat, ◇ 2.82 amagat, + 3.78 amagat.
FSR = 75.6 GHz; X 2.82 amagat, ◁ 3.78 amagat, ▷ 4.76 amagat.
The dashed line corresponds to the initial slope of the curve.
The points with FSR = 75.6 GHz have been obtained using an Argon laser operating at 5145 Å (see also chapter III).

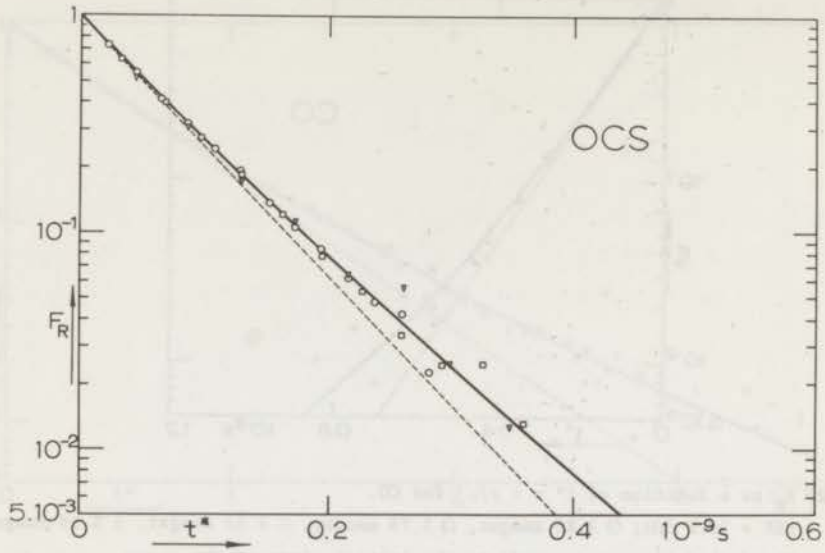

Fig. 14. F_R as a function of $t^* = t\,\rho/\rho_o$ for OCS.
FSR = 85.4 GHz; ○ 1.86 amagat, □ 2.80 amagat, ▽ 3.73 amagat.
The dashed line corresponds to the initial slope of the curve.

linear in the density over the investigated pressure range. Contributions to the line profile with a different density dependence are apparently negligible. Therefore the possibility can be excluded that the translational motion of the molecules (Doppler or diffusional width) has a significant effect on the line shape. Also contributions with time scales of the duration of a collision are absent. Likewise it indicates that no systematic errors have been made in applying corrections to the interferograms (section 3).

For nH_2 and pH_2 (figs. 8, 9) the shape of the curves is fairly well linear, indicating a Lorentzian line profile. The curves for HD, nD_2, N_2, CO, CO_2 and OCS on the other hand (figs. 7,10-14) show definitely that deviations from a Lorentz shape do occur. The conclusion that can be drawn from the present results is apparently that the collisional broadening of the depolarized Rayleigh line is in general not associated with a Lorentzian line shape. This result is in contradiction with the conclusions of previous studies[3,4,5]. We believe, however, that previously no deviations from a Lorentzian have been noticed in studies of

the depolarized Rayleigh line broadening for N_2 and CO_2 [3] and HD and nD_2 [5], due to the analyzing procedure followed by the authors. In fact they started out by assuming a Lorentzian shape for the depolarized Rayleigh line and convoluted this profile with the experimentally measured instrumental function. By varying height and half-width of the Lorentzian a best fit with the experimental spectrum was obtained. It will be clear that in such an approach small deviations from a Lorentz shape are not easily observed.

That no deviations were found in our previously reported investigation of the depolarized Rayleigh line for the gases CO_2 and OCS[4] was due to the relatively large corrections that had to be applied to the spectra in the early stage of the experiments.

A qualitative explanation of the occurrence of deviations from a Lorentzian profile can simply be given. For a particular gas all rotating molecules contribute to the depolarized Rayleigh line. Since the line broadening is caused by collisional reorientation of the molecules (see the introduction to this chapter), a dependence of the reorientation probability on the rotational state could give rise to deviations from a simple Lorentzian behavior. Such a rotational dependence seems very plausible from the point of view of gyroscopic stability. On the other hand, in a situation where the contributions to the depolarized Rayleigh line come mainly from one single rotational state ($j = 1$ for nH_2, $j = 2$ for pH_2), the departure is expected to be small and this is indeed observed. A more thorough discussion of this subject will be given in section 5).

4.2 Numerical results. For Lorentzian lines the linewidth $\Delta\nu_{\frac{1}{2}}$ (half-width at half intensity) is the characteristic parameter and experimental results on collisional broadening are usually presented in the form of a broadening coefficient $\Delta\nu_{\frac{1}{2}}/\rho$. In case the line shape deviates from a Lorentzian profile, however, $\Delta\nu_{\frac{1}{2}}$ is a rather arbitrary measure for the broadening. For the description of the collisional broadening of the depolarized Rayleigh line a more convenient choice is

a quantity Γ, with the dimension of frequency, related to the initial slope of $F_R(t)$:

$$2\pi\Gamma = -\left(\frac{dF_R}{dt}\right)_{t=0} \quad . \tag{9}$$

Another quantity of interest, which we will denote by $\tilde{\Gamma}$, is related to the time integral of $F_R(t)$:

$$(2\pi\tilde{\Gamma})^{-1} = \int_0^\infty F_R(t)\, dt \quad . \tag{10}$$

Since $(2\pi\tilde{\Gamma})^{-1}$ represents the area under the curve of $F_R(t)$ and $(2\pi\Gamma)^{-1}$ the area under the exponential with the same initial slope, the difference between Γ and $\tilde{\Gamma}$ is a measure for the departure from Lorentzian behavior. For a Lorentzian one has $\Gamma = \tilde{\Gamma} = \Delta\nu_{\frac{1}{2}}$. In general, however, Γ and $\tilde{\Gamma}$ are not simply related to a linewidth.

Table III

Experimental results at 293 K

	Γ/ρ (GHz/amagat)	$\tilde{\Gamma}/\rho$ (GHz/amagat)	$\frac{\Gamma - \tilde{\Gamma}}{\Gamma}$	$\Delta\nu_{\frac{1}{2}}/\rho$ (GHz/amagat)	
nH_2	0.0539 ± 0.0005	0.0531 ± 0.0005	0.01^5	0.053 ± 0.002	a)
pH_2	0.056 ± 0.001	0.056 ± 0.001	0.00	-	
HD	0.279 ± 0.005	0.257 ± 0.005	0.08	0.0238 ± 0.0006	a)
nD_2	0.079 ± 0.001	0.070 ± 0.001	0.11	0.070 ± 0.002	a)
N_2	0.98 ± 0.02	0.90 ± 0.02	0.08	0.81	b)
CO	1.22 ± 0.03	1.14 ± 0.03	0.06^5	-	
CO_2	2.01 ± 0.05	1.89 ± 0.05	0.06	1.8	b)
OCS	2.18 ± 0.05	2.05 ± 0.05	0.06	-	

A density of 1 amagat corresponds approximately to $2.687\ 10^{19}$ molecules/cm^3.

a) ref. 5

b) ref. 3

Γ/ρ and $\tilde{\Gamma}/\rho$ can be considered as broadening coefficients. Values for these broadening coefficients are extracted from the experimental curves of $F_R(t^*)$, using eqs. (9), (10) and (8). The results for the various gases are given in table III. Values for $(\Gamma - \tilde{\Gamma})/\Gamma$ are also given. It is seen that for the hydrogen isotopes the deviations from Lorentzian behavior increase from virtually zero for nH_2 and pH_2 to about 11% for nD_2. For the larger molecules, however, the deviations are smaller again. An illustration of the relative deviations for the hydrogen isotopes is given in fig. 15, where we have plotted, for nH_2, HD and D_2, the curves through the experimental points after having matched the initial slopes.

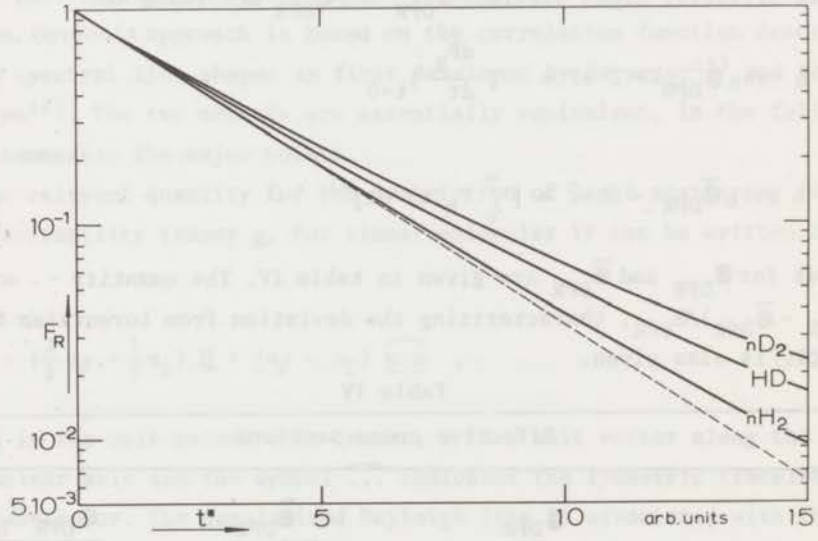

Fig. 15. The deviation from a Lorentzian shape of the depolarized Rayleigh line for the gases nH_2, HD and nD_2. The initial slopes of the curves of F_R for the three gases have been matched.

Values for $\Delta\nu_{\frac{1}{2}}/\rho$ as obtained in earlier investigations in which a Lorentzian line shape was assumed are also given in table III. For nH_2, where the line shape is Lorentzian within experimental error, a direct comparison can be made. The value for $\Delta\nu_{\frac{1}{2}}/\rho$ in this case is in excellent agreement with our results. For the other gases the previously reported values for $\Delta\nu_{\frac{1}{2}}/\rho$ are expected to be about the same as the here presented numbers, which is indeed the case.

The experimental broadening coefficients are usually expressed in terms of effective cross sections using the relation

$$n < v >_0 \mathfrak{S} = 2 \pi \Delta\nu_{\frac{1}{2}} \quad . \tag{11}$$

n is the number density and $<v>_0$ the average relative velocity

$$<v>_0 = \left(\frac{8 k_B T}{\pi \mu} \right)^{\frac{1}{2}} \quad , \tag{12}$$

where k_B is Boltzmann's constant, T the absolute temperature and μ the reduced mass of a pair of molecules.

In an analogous way we express now the quantities Γ and $\tilde{\Gamma}$ in terms of two effective cross sections $\mathfrak{S}_{DPR}$ and $\tilde{\mathfrak{S}}_{DPR}$ according to:

$$n <v>_0 \mathfrak{S}_{DPR} = 2 \pi \Gamma = - \left(\frac{dF_R}{dt} \right)_{t=0} \tag{13}$$

and

$$n <v>_0 \tilde{\mathfrak{S}}_{DPR} = 2 \pi \tilde{\Gamma} = \left[\int_0^\infty F_R(t)\, dt \right]^{-1} \quad . \tag{14}$$

Values for $\mathfrak{S}_{DPR}$ and $\tilde{\mathfrak{S}}_{DPR}$ are given in table IV. The quantity $(\mathfrak{S}_{DPR} - \tilde{\mathfrak{S}}_{DPR})/\mathfrak{S}_{DPR}$, characterizing the deviation from Lorentzian behavior, is also given.

Table IV

Effective cross sections

	$\mathfrak{S}_{DPR}$ (Å^2)	$\tilde{\mathfrak{S}}_{DPR}$ (Å^2)	$\frac{\mathfrak{S}_{DPR} - \tilde{\mathfrak{S}}_{DPR}}{\mathfrak{S}_{DPR}}$
nH_2	0.508 ± 0.005	0.500 ± 0.005	0.01^5
pH_2	0.53 ± 0.01	0.53 ± 0.01	0.00
HD	3.21 ± 0.06	2.95 ± 0.05	0.08
nD_2	1.05 ± 0.02	0.93 ± 0.02	0.11
N_2	34.4 ± 0.6	31.6 ± 0.6	0.08
CO	43 ± 1	40 ± 1	0.06^5
CO_2	88 ± 2	83 ± 2	0.06
OCS	112 ± 2	105 ± 2	0.06

It is noted that the cross section values for HD are considerably larger than those for the other hydrogen isotopes. Such a trend is also observed in various other experiments[30,31]. It is attributed to the strong asymmetry in the mass distribution of the HD molecule ("loaded sphere"), which gives rise to a strong angle-dependent term in the interaction between HD molecules. The detailed theoretical significance of the cross sections will be discussed in the next section.

5. Theory and discussion. 5.1 General. The theory for the broadening of the depolarized Rayleigh line in dilute gases of linear molecules was developed by Hess[32,33] and Gordon[2,34]. The approach of Hess is a kinetic one: relaxation equations are derived from the Waldmann-Snider equation. Gordon's approach is based on the correlation function description of spectral line shapes as first developed by Baranger[35] and Kolb and Griem[36]. The two methods are essentially equivalent. In the following we summarize the major points.

The relevant quantity for the description of light scattering is the polarizability tensor $\underline{\underline{\alpha}}$. For linear molecules it can be written in the form

$$\underline{\underline{\alpha}} = (\tfrac{2}{3}\alpha_{/\!/} + \tfrac{1}{3}\alpha_{\perp})\,\underline{\underline{U}} + (\alpha_{/\!/} - \alpha_{\perp})\,\overbrace{\underline{u}\,\underline{u}}\,, \qquad (15)$$

where $\underline{\underline{U}}$ is the unit second rank tensor, $\underline{u}$ is a unit vector along the internuclear axis and the symbol $\overbrace{\ldots}$ indicates the symmetric traceless part of a tensor. The depolarized Rayleigh line is associated with that part of the tensor operator $\overbrace{\underline{u}\,\underline{u}}$ that is diagonal in the rotational quantum number j. This part, $\overbrace{\underline{u}\,\underline{u}}\,(\underline{J})$, is related to the tensor $\overbrace{\underline{J}\,\underline{J}}$ by

$$\overbrace{\underline{u}\,\underline{u}}\,(\underline{J}) = -\tfrac{1}{2}\,\frac{\overbrace{\underline{J}\,\underline{J}}}{J^2 - \frac{3}{4}}\,. \qquad (16)$$

Due to orientational fluctuations the local instantaneous mean value of this tensor is in general nonzero and this gives rise to the occurrence of depolarized Rayleigh light scattering. The depolarized Rayleigh line

profile is determined by the correlation function C (t), describing the decay of these fluctuations:

$$C(t) = \frac{\sum_{\ell,m} < \frac{\overbrace{J_\ell J_\ell}}{J_\ell^2 - \frac{3}{4}}(0) : \frac{\overbrace{J_m J_m}}{J_m^2 - \frac{3}{4}}(t) >_0}{\sum_{\ell} < \frac{\overbrace{J_\ell J_\ell}}{J_\ell^2 - \frac{3}{4}}(0) : \frac{\overbrace{J_\ell J_\ell}}{J_\ell^2 - \frac{3}{4}}(0) >_0} \qquad (17)$$

The brackets $<.....>_0$ denote a statistical average. Different molecules are labeled by indices ℓ and m. At low densities where the translational motion of the molecules is important, the correlation function depends also on the scattering wave vector $\underline{k}$. At higher densities, however, only collisional reorientation effects are important and the dependence on $\underline{k}$ disappears. Since we are only concerned with the latter case we will ignore the $\underline{k}$ dependence in our discussion.

The spectral function $R(\nu)$ describing the depolarized line profile is related to C (t) by

$$C(t) = \frac{1}{I_0} \int_{-\infty}^{+\infty} R(\nu)\, e^{-i2\pi\nu t}\, dt \quad . \qquad (18)$$

We see at this point that the experimentally obtained quantity $F_R(t)$ (see section 3.7) can be identified with the correlation function C (t):

$$F_R(t) = C(t) \quad . \qquad (19)$$

5.2 Discussion of various theoretical models. The crucial theoretical point is the form of the explicit expression for the correlation function C(t). Different expressions have been obtained by Hess[32,33] (I), McCourt *et al.*[37] (II) and Shafer and Gordon[38] (III). We will discuss the three approaches and then, in the next section, compare the results with the observed experimental behavior.

I) Hess's treatment is the most simple one. It assumes that the decay of $\underline{\overbrace{J\,J}}/(J^2 - \frac{3}{4})$ polarization (second rank orientational polarization) can be described with one rate coefficient (one-moment approximation).

Consequently, the correlation function C(t) has the form of a simple exponential:

$$C(t) = e^{-n\langle v\rangle_0 \, \mathfrak{S}(0\hat{2})\, t} \quad , \tag{20}$$

with the effective reorientation cross section* $\mathfrak{S}(0\hat{2})$ related to the collision integral for orientational polarization by

$$\mathfrak{S}(0\hat{2}) = \frac{1}{\langle v\rangle_0} \frac{\left\langle \dfrac{\overbrace{\underline{J}\,\underline{J}}}{J^2 - \frac{3}{4}} : R_0 \dfrac{\overbrace{\underline{J}\,\underline{J}}}{J^2 - \frac{3}{4}} \right\rangle_0}{\left\langle \dfrac{\overbrace{\underline{J}\,\underline{J}}}{J^2 - \frac{3}{4}} : \dfrac{\overbrace{\underline{J}\,\underline{J}}}{J^2 - \frac{3}{4}} \right\rangle_0} \quad . \tag{21}$$

R_0 is the collision operator used in the Waldmann-Snider equation:

$$R_0\,\phi = -(2\pi)^4 \hbar^2 n^{-1} \, \mathrm{tr}_1 \int d\underline{p}_1 \, f_1^{(0)} \{ \int t^{g}_{g'}(\phi' + \phi_1')\, t^{g^\dagger}_{g''} \, \delta(E)\, d\underline{p}' - \frac{i}{2\pi} [\, t^{g}_{g}(\phi + \phi_1) - (\phi + \phi_1)\, t^{g^\dagger}_{g}] \} \quad . \tag{22}$$

For the meaning of the various symbols see ref. 40.

II) In a more complicated description it is assumed that the polarization in each rotational manifold has its own decay rate. This so-called uncoupled model was introduced by Coope and Snider[41] and worked out for depolarized Rayleigh scattering by McCourt *et al.*[37]. It leads to the introduction of an effective cross section for reorientation σ_j for each individual j state. As a consequence, C(t) is a sum of exponentials weighted over the various rotational states:

$$C(t) = \frac{\sum_j p_j \, d_j^{\,2} \, e^{-n\,\langle v\rangle_0\, \sigma_j t}}{\sum_j p_j \, d_j^{\,2}} \quad , \tag{23}$$

* The notation $\mathfrak{S}(02)$ is commonly used for the cross section for decay of $\overbrace{\underline{J}\,\underline{J}}$ polarization[39]. We write $\hat{2}$ instead of 2 to indicate a description in terms of $\overbrace{\underline{J}\,\underline{J}}/(J^2 - \frac{3}{4})$.

where p_j is the fractional population of rotational state j and d_j a weighting factor given by

$$d_j = \left(\frac{J^2}{4J^2 - 3}\right)^{\frac{1}{2}} = \left[\frac{j(j+1)}{(2j-1)(2j+3)}\right]^{\frac{1}{2}} . \qquad (24)$$

III) Gordon[34,38] developed a model in which coupling between rotational levels is also included, *i.e.*, collisions can transfer orientational polarization from one rotational state to another. In this situation the correlation function C(t) has the following form[38]:

$$C(t) = \frac{\sum_{i,j} p_j \, d_i d_j \, (e^{-n \langle v \rangle_0 \, \underline{\sigma} \, t})_{ij}}{\sum_j p_j \, d_j^2} . \qquad (25)$$

$\underline{\sigma}$ is a cross section matrix, of which the diagonal elements σ_{jj} describe the decay of orientational polarization in rotational state j, while the off-diagonal elements σ_{ij} determine the transfer of polarization from state j to state i.

It is obvious that case III reduces to case II if one sets the transfer coefficients $\sigma_{ij} = 0$ $(i \neq j)$. Furthermore, the correlation functions for case II and III take the form of a simple exponential (case I) when only one rotational level is involved. For the uncoupled model this is also the case when the decay coefficients σ_j are independent of j. Finally, case III reduces to case I in the limit of infinitely strong coupling.

It should be pointed out that a multi-moment description, within the framework of a kinetic approach as used by Hess, would be fully equivalent to Shafer and Gordon's method, provided a complete set of polarizations is used. Note, moreover, that in such a multi-moment approach the initial slope of the correlation function is still determined by the cross section $\mathfrak{S}(0\hat{2})$, corresponding to the first moment $\overline{\underline{J}\,\underline{J}}/(J^2 - \frac{3}{4})$ (see ref. 42). Hence the cross section $\mathfrak{S}(0\hat{2})$ defined in eq. (21) can directly be related to the cross section matrix $\underline{\sigma}$ ocurring in eq.(25):

$$\mathfrak{S}(0\hat{2}) = \frac{\sum_{i,j} p_j \, d_i \, d_j \, \sigma_{ij}}{\sum_j p_j \, d_j^2} \quad . \tag{26}$$

For a comparison with the experimental results one needs the relation between theoretical and experimental quantities. We have seen already (eq. (19)), that the theoretical correlation function C(t) can be identified with the experimentally obtained Fourier transform $F_R(t)$. From eq. (25) one obtains now the following theoretical expressions for the cross sections $\mathfrak{S}_{DPR}$ and $\tilde{\mathfrak{S}}_{DPR}$, which characterize the initial slope and the time integral of the experimental correlation function (eqs. (13) and (14)):

$$\mathfrak{S}_{DPR} = \frac{\sum_{i,j} p_j \, d_i d_j \, \sigma_{ij}}{\sum_j p_j \, d_j^2} = \mathfrak{S}(0\hat{2}) \tag{27}.$$

and

$$\tilde{\mathfrak{S}}^{-1}_{DPR} = \frac{\sum_{i,j} p_j \, d_i d_j \, (\underline{\sigma}^{-1})_{ij}}{\sum_j p_j \, d_j^2} \quad . \tag{28}$$

Both $\mathfrak{S}_{DPR}$ and $\tilde{\mathfrak{S}}_{DPR}$ have to be considered as effective reorientation cross sections. Comparison of eqs. (27) and (28) shows that, where $\mathfrak{S}_{DPR}$ determines the average decay rate, $\tilde{\mathfrak{S}}_{DPR}$ is, in fact, related to an average decay time.

5.3 Comparison between theory and experiment. The experimentally obtained correlation functions for nH_2 and pH_2 (figs. 8,9) are in good approximation single exponential curves, so that eq. (20) gives a good description. For nH_2 and pH_2 at roomtemperature one observes essentially only molecules in, respectively, the j=1 and j=2 states, so that a decay with only one relaxation time is not surprising. For HD, nD_2, N_2, CO, CO_2, and OCS, molecules for which more rotational states contribute, distinct deviations from a single exponential decay are observed (figs. 7,10-14).

The uncoupled model (eq. (23)) could account for such deviations from single exponential behavior, but in order to make a comparison possible an explicit expression for the j-dependence of the cross sections σ_j is needed. In the distorted wave Born approximation it is found[43,44] that for a P_2-type of interaction σ_j is roughly proportional to j^{-2}:

$$\sigma_j = \frac{4\ (4j^2+4j-7)}{(2j-1)^2(2j+3)^2}\ \sigma^{(o)} \qquad (29)$$

with $\sigma^{(o)}$ a cross section that is independent of j. Using eqs. (13), (14), (19) and (23) one obtains now the following theoretical expressions for the cross sections $\mathfrak{S}_{DPR}$ and $\tilde{\mathfrak{S}}_{DPR}$:

$$\mathfrak{S}_{DPR} = \frac{\sum_j p_j\ d_j^2\ \frac{4\ (4j^2+4j-7)}{(2j-1)^2(2j+3)^2}}{\sum_j p_j\ d_j^2}\ \sigma^{(o)} \qquad (30)$$

and

$$\tilde{\mathfrak{S}}^{-1}_{DPR} = \frac{\sum_j p_j\ d_j^2\ \frac{(2j-1)^2(2j+3)^2}{4(4j^2+4j-7)}}{\sum_j p_j\ d_j^2}\ \sigma^{(o)-1}\ . \qquad (31)$$

As a measure for the departure from single exponential (Lorentzian) behavior, the quantity $(\mathfrak{S}_{DPR} - \tilde{\mathfrak{S}}_{DPR})/\mathfrak{S}_{DPR}$ is calculated theoretically for the various gases, using eqs. (30) and (31). The results are shown in table V together with the values as obtained from the experiments. For nH_2 and pH_2 the values for $(\mathfrak{S}_{DPR} - \tilde{\mathfrak{S}}_{DPR})/\mathfrak{S}_{DPR}$ are small, both theoretically and experimentally, as should be expected in a situation where only one j state is important. For HD, where more rotational states contribute, the agreement seems very good. This can also be seen from fig. 16, where the full theoretical correlation function for HD is compared with the experimental one. The initial slope of the theoretical curve has been fitted to that of the experimental curve by adjusting the constant $\sigma^{(o)}$ in eq. (29). However, this agreement is probably accidental, since for the very asymmetric HD molecule the assumption of a P_2-type of potential is certainly invalid. For the heavier molecules, on the

Table V

Comparison of experimental results with the uncoupled model (see eq. (23))

	$\frac{\mathcal{E}_{DPR}-\tilde{\mathcal{E}}_{DPR}}{\mathcal{E}_{DPR}}$	
	experiment	uncoupled model with σ_j as given by eq. (29)
nH_2	0.01[5]	0.03[5]
pH_2	0.00	0.04
HD	0.08	0.07
nD_2	0.11	0.17
N_2	0.08	0.70
CO	0.06[5]	0.71
CO_2	0.06	0.80
OCS	0.06	0.83
very heavy linear molecule	-	1

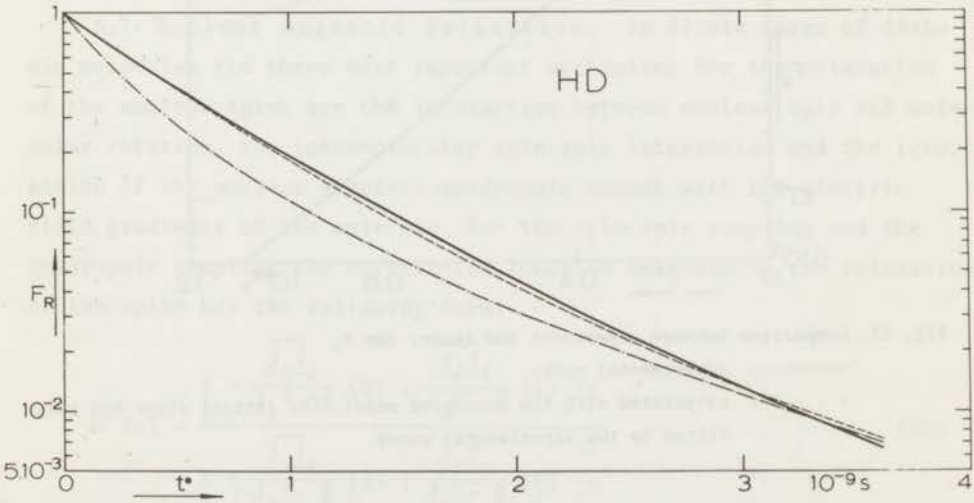

Fig. 16. Comparison between experiment and theory for HD.

———— experimental curve.

- - - - - calculated with the uncoupled model. The initial slope has been fitted to the experimental curve.

- · - · - semiclassical calculation of Gordon *et al.*[45].

other hand, where a P_2-type of interaction may be expected to give a good description, there exists distinct disagreement with the experimental behavior. Again this is illustrated in detail in fig.17, showing the experimental and theoretical correlation functions for N_2. Apparently the uncoupled model with a j-dependent decay cross section as given by eq. (29) is an unsatisfactory approach. This might be due to the assumption of a P_2-type of interaction or to the distorted wave Born approximation. However, it seems most likely that there is a considerable transfer of polarization between different rotational states, especially for the larger molecules, so that a description in terms of uncoupled rotational manifolds is not valid.

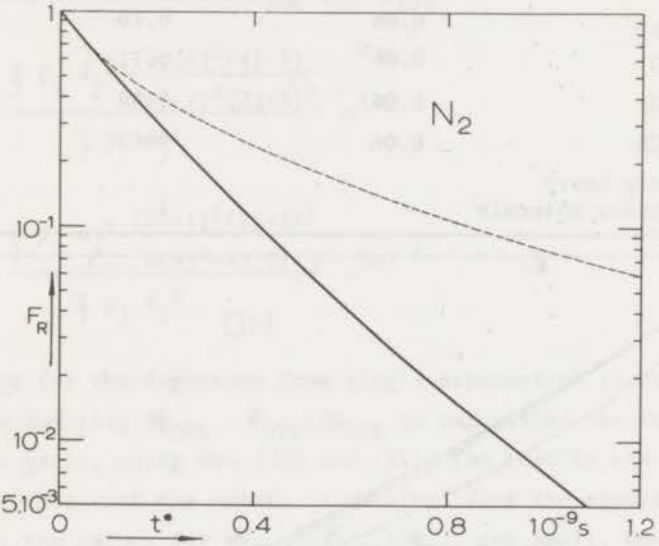

Fig. 17. Comparison between experiment and theory for N_2.
———— experimental curve.
- - - - - calculated with the uncoupled model. The initial slope has been fitted to the experimental curve.

This leads then to the conclusion that for a good description of the experimental results the most general form of the correlation function (eq. (25)) has to be used. For a calculation of this function one has to know the complete cross section matrix $\underline{\sigma}$. An explicit quantum

mechanical calculation of the matrix elements σ_{ij} has thus far only been performed for the system H_2-He [38]. The calculated correlation function in this case is very nearly exponential. For HD an approximative form of the cross section matrix has been obtained along semiclassical lines[45]. The resulting correlation function C(t) is shown in fig. 16. The discrepancy with the experimental curve is rather large, but this may be due to the fact that the semiclassical approach is in error for very low j values, which give an important contribution in HD. One should note, however, that this theoretical curve for HD does not contain an adjustable parameter, as is the case for the curve representing the uncoupled model.

6. Comparison with other experiments. Cross sections related to molecular reorientation are also obtained from experiments on nuclear magnetic relaxation (NMR) and from the Senftleben-Beenakker (SB) effect for the viscosity. In this section we discuss in how far these cross sections can be compared with cross sections obtained from depolarized Rayleigh line broadening.

6.1 Nuclear magnetic relaxation. In dilute gases of diatomic molecules the three most important mechanisms for the relaxation of the nuclear spins are the interaction between nuclear spin and molecular rotation, the intramolecular spin-spin interaction and the interaction of the nuclear electric quadrupole moment with the electric field gradients of the molecule. For the spin-spin coupling and the quadrupole coupling the correlation function determining the relaxation of the spins has the following form:

$$C'(t) = \frac{\sum_{\ell} < \frac{\overrightarrow{J_\ell J_\ell}}{J_\ell^{2-\frac{3}{4}}}(0) : \frac{\overrightarrow{J_\ell J_\ell}}{J_\ell^{2-\frac{3}{4}}}(t) >_0}{\sum_{\ell} < \frac{\overrightarrow{J_\ell J_\ell}}{J_\ell^{2-\frac{3}{4}}}(0) : \frac{\overrightarrow{J_\ell J_\ell}}{J_\ell^{2-\frac{3}{4}}}(0) >_0} \quad . \tag{32}$$

This correlation function is almost identical to the one determining the depolarized Rayleigh line (eq. (17)). The difference is that for NMR only self-correlations are considered. This is a consequence of the assumption that collisions by themselves do not change spin states.

In the case that a nuclear quadrupole moment is present, *i.e.*, for nuclear spin greater than $\frac{1}{2}$, the quadrupole coupling is the dominant relaxation mechanism and the other two mechanisms may be ignored. Two different cases have to be distinguished: a) only one of the nuclei possesses a quadrupole moment and b) both nuclei are identical and have spins greater than $\frac{1}{2}$. Only the extreme narrowing limit will be considered. In case a) the expression for the spin relaxation time obtains the following form[38]:

$$T_1^{-1} = \frac{3}{40} \frac{2I_1 + 3}{I_1^2 (2I_1 - 1)} \left(\frac{eq\ Q}{\hbar} \right)^2 \sum_{i,j} P_j\, d_i d_j\, (\underline{\sigma}'^{-1})_{ij} \,. \qquad (33)$$

Here I_1 is the spin of the relevant nucleus and $(eq\ Q)/\hbar$ is the quadrupole coupling constant; d_i and d_j are defined by eq. (24). This case applies, for example, to the deuteron resonance in HD where one has $I_1 = 1$. The difference between the cross section matrix $\underline{\sigma}'$ that occurs here and the cross section matrix $\underline{\sigma}$ determining the broadening of the depolarized Rayleigh line is that the collision partner does not explicitely occur in the formal expression for a matrix element σ'_{ij}.

An effective cross section $\tilde{\mathfrak{S}}'_Q$ can now be introduced according to:

$$T_1^{-1} = \frac{3}{40} \frac{2I_1 + 3}{I_1^2 (2I_1 - 1)} \left(\sum_j p_j\, d_j^2 \right) \left(\frac{eq\ Q}{\hbar} \right)^2 \left(n \langle v \rangle_0\, \tilde{\mathfrak{S}}'_Q \right)^{-1} \qquad (34)$$

$\tilde{\mathfrak{S}}'_Q$ is related to the cross section matrix elements σ'_{ij} by

$$\left(\tilde{\mathfrak{S}}'_Q \right)^{-1} = \frac{\sum_{i,j} p_j\, d_i d_j\, (\underline{\sigma}'^{-1})_{ij}}{\sum_j p_j\, d_j^2} \qquad (35)$$

Note that this expression is identical to the one for $\tilde{\mathfrak{S}}^{-1}_{DPR}$ (eq. (28)) except for the prime.

For homonuclear molecules (case b) transitions between odd and even rotational states are forbidden and the system may be considered as a mixture of ortho and para species. Two spin relaxation times occur in that situation. Bloom[46] has considered the case of $I_1 = 1$ which can be described as follows:

$$T_1^{-1}{}_{\text{ortho}} = \frac{3}{8}\left(\frac{eqQ}{\hbar}\right)^2 \frac{1}{n\,\langle v\rangle_0} \sum_{i,j\ \text{even}} p_j\, d_i d_j\, (\underline{\sigma}'^{-1})_{ij} \qquad (36)$$

$$T_1^{-1}{}_{\text{para}} = \frac{3}{8}\left(\frac{eqQ}{\hbar}\right)^2 \frac{1}{n\,\langle v\rangle_0} \sum_{i,j\ \text{odd}} p_j\, d_i d_j\, (\underline{\sigma}'^{-1})_{ij} \qquad (37)$$

Also here effective cross sections $\tilde{\sigma}'_Q$ can be introduced in a way analogous to eq. (34). General expressions for T_1, valid for any I_1, have recently been given by Sanctuary[47]. The case $I_1 = 1$ applies to D_2 and N_2. In NMR studies on these molecules at room temperature only one single relaxation time was observed, which is attributed mainly to the ortho species[48].

Values for $\tilde{\sigma}'_Q$ have been extracted from NMR experiments on HD and nD_2 [48], and on N_2 [49]. The results are given in table VI together with the values for the depolarized Rayleigh cross sections. From eq. (28) and (35) one can see that the effective cross section $\tilde{\sigma}'_Q$, obtained in the extreme narrowing limit, has to be compared with the cross section $\tilde{\sigma}_{DPR}$. The difference between these two cross sections is a direct measure for the transfer of orientational polarization between the colliding molecules. If such an effect were present, one would expect $\tilde{\sigma}'_Q$ to be larger than $\tilde{\sigma}_{DPR}$. From the fact that $\tilde{\sigma}'_Q$ is larger for D_2 (by 7%) but smaller for HD and N_2 (by 15%) it can be concluded that the observed differences are probably due to inaccuracies in the NMR cross sections. It should also be pointed out that the NMR relaxation for N_2 was carried out at very high densities (100-600 amagat) where the gas can no longer be considered as dilute. Before a definite conclusion can be made, more accurate NMR data (for N_2 also at lower densities) are needed.

For nH_2 comparison of $\tilde{\sigma}_{DPR}$ with an effective cross section obtained from spin-spin relaxation would be possible. This spin-spin contribution, however, always occurs together with a relaxation due to spin-rotation coupling. For H_2 a reliable separation of these two contributions has not yet been successfully accomplished and therefore a straightforward comparison cannot be made.

Table VI

Comparison of effective cross sections from different experiments

	$\mathcal{S}_{DPR}$ (Å^2)	$\tilde{\mathcal{S}}_{DPR}$ (Å^2)	$\tilde{\mathcal{S}}'_Q$ (Å^2)	$\mathcal{S}_{SB}$ (Å^2)
nH_2	0.508 ± 0.005	0.500 ± 0.005		0.54 ± 0.06 c)
pH_2	0.53 ± 0.01	0.53 ± 0.01		0.50 ± 0.05 c)
HD	3.21 ± 0.06	2.95 ± 0.05	2.5 a)	2.26 ± 0.07 d)
nD_2	1.05 ± 0.02	0.93 ± 0.02	1.0 a)	0.86 ± 0.08 c)
N_2	34.4 ± 0.06	31.6 ± 0.6	27 b)	23.7 ± 0.09 d)
CO	43 ± 1	40 ± 1		32.5 ± 0.08 d)
CO_2	88 ± 2	83 ± 2		69 ± 1.5 e)

a) ref. 48
b) ref. 49
c) ref. 52
d) ref. 39
e) ref. 6

6.2 The Senftleben-Beenakker effect for the viscosity. Another way to probe molecular reorientation in dilute polyatomic gases is to investigate the viscosity change in a magnetic field. The external field, through its interaction with the rotational magnetic moment of the molecules, causes a precession of the rotational angular momenta. When the precession frequency becomes of the order of the collisional reorientation frequency a change of the viscosity coefficients is observed[50,51]. It is found that the relative change in the viscosity, $\Delta\eta_1^+/\eta$ can in good approximation be described with a single relaxation time[6-8,31,39]:

$$-\frac{\Delta\eta_1^+}{\eta} = \Psi \frac{\omega_L^2 \tau^2}{1 + \omega_L^2 \tau^2} \quad . \tag{38}$$

Ψ describes the magnitude of the viscosity change and τ is the relaxation time. The Larmor precession frequency ω_L is given by

$$\omega_L = \frac{g\,\mu_N\,H}{\hbar} \quad . \tag{39}$$

H is the magnetic field, g the molecular g factor and μ_N the nuclear magneton. For the notation of the various viscosity coefficients see ref. 39. From the relaxation time τ an effective cross section $\mathfrak{S}_{SB}$ is obtained in the usual way:

$$\frac{1}{\tau} = n\,\langle v\rangle_0\,\mathfrak{S}_{SB} \quad . \tag{40}$$

Values for $\mathfrak{S}_{SB}$ have been determined for most of the gases for which we investigated the depolarized Rayleigh line (see table VI).

In the description of the SB effect for the viscosity, $\mathfrak{S}_{SB}$ is usually identified with a cross section $\mathfrak{S}(02)$:

$$\mathfrak{S}_{SB} = \mathfrak{S}(02) = \frac{1}{\langle v\rangle_0}\,\frac{\langle \overbrace{\underline{J}\,\underline{J}} : R_0\,\overbrace{\underline{J}\,\underline{J}}\rangle_0}{\langle \overbrace{\underline{J}\,\underline{J}} : \overbrace{\underline{J}\,\underline{J}}\rangle_0} \tag{41}$$

This implies that one assumes that the dominant polarization is of the form $\overbrace{\underline{J}\,\underline{J}}$. However, other expansion terms of the same tensorial character, such as, *e.g.*, $\overbrace{\underline{J}\,\underline{J}}/(J^2 - \frac{3}{4})$, describe equally well the experimentally observed field dependence as represented by eq. (38). From the SB experiments themselves no answer can be obtained to the question as to what would be the proper choice for the first expansion term.

Although the cross section $\mathfrak{S}_{SB}$ can as yet not be properly identified it should be of the same order as $\mathfrak{S}_{DPR}$ ($= \mathfrak{S}(0\hat{2})$. This is indeed observed. On the other hand, from the fact that $\mathfrak{S}_{DPR}$ is, especially, for the heavier gases, considerably larger than $\mathfrak{S}_{SB}$, it can be concluded that a description in terms of $\overbrace{\underline{J}\,\underline{J}}/(J^2 - \frac{3}{4})$ is not appropriate for the SB effect. In fact $\overbrace{\underline{J}\,\underline{J}}$ might be a better choice as it gives more weight to the higher j-values. Assuming that the reorientation probability decreases with increasing j, this would indeed lead to a smaller value for the SB cross section. The distinction between $\overbrace{\underline{J}\,\underline{J}}$,

$\overbrace{\underline{J}\,\underline{J}}/(J^2 - \frac{3}{4})$ and other similar polarizations is of course meaningless when only one single j level is involved. In that situation the corresponding cross sections $\mathfrak{S}(02)$, $\mathfrak{S}(0\hat{2})$, *etc.* are all identical. Hence the experimental cross sections $\mathfrak{S}_{SB}$ and $\mathfrak{S}_{DPR}$ should be equal for nH_2 (j=1) and pH_2 (j=2). Recent viscosity experiments for those gases[52] indicated that this is indeed the case (see table VI). Previously reported SB results for nH_2 and pH_2 [31] were shown to be in error.

A definite solution to the problem of the proper description of the SB effect for gases for which more rotational levels contribute, can only be obtained from a careful theoretical investigation of the convergence of the various possible expansion series and a calculation of the corresponding cross sections for a realistic potential. Such an investigation has thusfar been carried out for a rough sphere model only[53]. For rough spheres, however, the reorientation probability does not at all depend on the molecular angular momentum and therefore this model is rather unrealistic for the description of polarizations of the type discussed here.

In several studies on the SB effect for the viscosity[6-8] small deviations have been found from the simple behavior described by eq. (38). One has tried to explain such deviations by attributing them to contributions with a different tensorial character such as $\overbrace{\underline{W}\,\underline{W}}\,\underline{J}$ and $\overbrace{\underline{W}\,\underline{W}}\,\overbrace{\underline{J}\,\underline{J}}$ ($\underline{W}$ is the peculiar velocity). However, these deviations may also be connected, as is the case for the depolarized Rayleigh line, with the fact that the molecular reorientation probabilities are j-dependent. In the usual description of the SB effect this would correspond to the occurrence of more terms of the expansion series of type $\overbrace{\underline{J}\,\underline{J}}$, *e.g.*, $\underline{J}\,\overbrace{\underline{J}}$, $(J^2-1)\overbrace{\underline{J}\,\underline{J}}$ *etc.* (see also ref. 8). A description in terms of a cross section matrix, analogous to the one used for the depolarized Rayleigh line, seems useful when only a few rotational states are populated.

References

1. Anderson, P.W., Phys. Rev. *76* (1949) 647.
2. Gordon, R.G., J. Chem. Phys. *44* (1966) 3083.
3. Cooper, V.G., May, A.D., Hara, E.H. and Knaap, H.F.P., Phys. Letters *27A* (1968) 52; IEEE J. Quantum Electron. *4* (1968) 720.
4. Keijser, R.A.J., Jansen, M.A., Cooper, V.G. and Knaap, H.F.P., Physica *51* (1971) 593.
5. Gupta, B.K. and May, A.D., Can. J. Phys. *50* (1972) 1747.
6. Korving, J., Physica *50* (1970) 27.
7. Hulsman, H., Van Waasdijk, E.J., Burgmans, A.L.J., Knaap, H.F.P. and Beenakker, J.J.M., Physica *50* (1970) 53.
8. Hulsman, H., Van Kuik, F.G., Walstra, K.W., Knaap, H.F.P. and Beenakker, J.J.M., Physica *57* (1972) 501.
9. Keijser, R.A.J., Van Den Hout, K.D. and Knaap, H.F.P., Phys. Letters *42A* (1972) 109.
10. Buckingham, A.D. and Disch, R.L., Proc. Roy. Soc. (London) Ser. A *273* (1963) 275.
11. Fookson, A., Pomerantz, P. and Rich, E.H., J. Res. Natl. Bur. Std. *47* (1951) 31.
12. Bridge, N.J. and Buckingham, A.D., Proc. Roy. Soc. (London) Ser. A *295* (1966) 334.
13. Landolt-Börnstein, Zahlenwerte und Funktionen (Springer-Verlag, Berlin, 1962), Band II, Part 8.
14. Hermans, L.J.F., De Groot, J.J., Knaap, H.F.P. and Beenakker, J.J.M., Physica *31* (1965) 1567.
15. Kolos, W. and Wolniewicz, L., J. Chem. Phys. *46* (1967) 1426.
16. Scharpen, L.H., Muenter, J.S. and Laurie, V.W., J. Chem. Phys. *53* (1970) 2513.
17. Butcher, R.J., Willets, D.V. and Jones, W.J., Proc. Roy. Soc. (London) Ser. A *324* (1971) 231.
18. Jones, G. and Gordy, W., Phys. Rev. A *135* (1964) 295.
19. Jammu, K.S., St.John, G.E. and Welsh, H.L., Can. J. Phys. *44* (1966) 797.

20. Placzek, G. and Teller, E., Z. Physik *81* (1933) 209; see also Herzberg, G., Molecular Spectra and Molecular Structure (D. Van Nostrand Company Inc., Princeton, 1950) Vol. 1.
21. Courtoy, C.P., Can. J. Phys. *35* (1957) 608.
22. Callomon, J.H. and Thompson, H.W., Proc. Roy. Soc. (London) Ser. A *222* (1954) 431.
23. Thibeau, M., Oksengorn, B. and Vodar, B., J. Phys. (Paris) *29* (1968) 287.
24. McTague, J.P. and Birnbaum, G., Phys. Rev. A *3* (1971) 1376.
25. Irwin, D.J.G. and May, A.D., Can. J. Phys. *50* (1972) 2174.
26. Kielich, S., Acta Phys. Polon. *19* (1960) 149.
27. Trappeniers, N.J., Kuz, V.A. and Ten Seldam, C.A., Physica *57* (1972) 294.
28. Cooper, V.G., Appl. Opt. *10* (1972) 525.
29. This thesis, chapter III; Keijser, R.A.J. *et al.*, Physica, to be published.
30. Prangsma, G.J., Heemskerk, J.P.J., Knaap, H.F.P. and Beenakker, J.J.M., Physica *50* (1970) 433.
31. Korving, J., Hulsman, H., Scoles, G., Knaap, H.F.P. and Beenakker, J.J.M., Physica *36* (1967) 177.
32. Hess, S., Z. Naturforsch. *24a* (1969) 1675; *25a* (1970) 350.
33. Hess, S., Springer Tracts Mod. Phys. *54* (1970) 136.
34. Gordon, R.G., J. Chem. Phys. *45* (1966) 1649.
35. Baranger, M., Phys. Rev. *111* (1958) 481; *112* (1958) 855.
36. Kolb, A.C. and Griem, H., Phys. Rev. *111* (1958) 514.
37. McCourt, F.R., Rudensky, T. and Moraal, H., Can. J. Phys. *51* (1973) 1627.
38. Shafer, R. and Gordon, R.G., J. Chem. Phys. *58* (1973) 5422.
39. Burgmans, A.L.J., Van Ditzhuyzen, P.G., Knaap, H.F.P. and Beenakker, J.J.M., Z. Naturforsch. *28a* (1973) 835.
40. Levi, A.C., McCourt, F.R. and Tip, A., Physica *39* (1968) 165.
41. Coope, J.A.R. and Snider, R.F., J. Chem. Phys. *56* (1972) 2049.
42. Hess, S. and Vestner, H., Z. Naturforsch. *28a* (1973) 1385.
43. McCourt, F.R. and Moraal, H., Phys. Rev. A *5* (1972) 2000.

44. Chen, F.M., Moraal, H. and Snider, R.F., J. Chem. Phys. *57* (1972) 542.

45. Gordon, R.G., Malone, J. and Knaap, H.F.P., to be published.

46. Bloom, M., M.T.P. International Review of Science, Physical Chemistry Section (Medical and Technical Publishing Company, Oxford, 1973) Vol. 4.

47. Sanctuary, B.C., Can. J. Phys. (1973) in press.

48. Hardy, W.N., thesis Vancouver (1964).

49. Speight, P.A. and Armstrong, R.L., Can. J. Phys. *47* (1969) 1475.

50. Beenakker, J.J.M., Festkörperprobleme VIII, (O. Madelung, Vieweg Verlag, Braunschweig, 1968) p. 276.

51. Beenakker, J.J.M. and McCourt, F.R., Ann. Rev. Phys. Chem. *21* (1970) 47.

52. Van Ditzhuyzen, P.G., private communication.

53. Moraal, H., McCourt, F.R. and Knaap, H.F.P., Physica *45* (1969) 455.

CHAPTER II

THE PRESSURE BROADENING OF THE DEPOLARIZED RAYLEIGH LINE: N_2 - NOBLE GAS MIXTURES

1. Introduction. The pressure broadening of the depolarized Rayleigh line in gases consisting of linear molecules measures the reorientation of rotational angular momentum in collisions[1-3] and thus probes the anisotropic part of the intermolecular potential. In chapter I[4], experiments have been reported on depolarized Rayleigh line broadening in pure gases. In this chapter, results are presented regarding the broadening of the depolarized Rayleigh line of N_2 in mixtures with the noble gases He, Ne and Ar at room temperature. This extension of experiments on the collisional broadening of the depolarized Rayleigh line to binary mixtures is desirable, since the description of the interaction between a nonspherical and a spherical particle is much simpler than the interaction between two nonspherical particles.

The broadening of the depolarized Rayleigh line is characterized by a correlation function C(t). For diatomic-monatomic gas mixtures this correlation function describes the decay of $\overline{\underline{J}\,\underline{J}}/(J^2 - \frac{3}{4})$ polarization (orientational polarization) of the diatomic molecules through collisions with both diatomic and noble gas molecules ($\underline{J}$ is the rotational angular momentum). In experiments, the correlation function can be obtained directly from a Fourier transformation of the recorded spectrum of the depolarized Rayleigh line. From the experimentally determined correlation functions effective cross sections can be extracted that measure the efficiency with which the diatomic molecules are reoriented by noble gas atoms. Values for such cross sections are presented for the systems N_2-He, N_2-Ne and N_2-Ar. They are compared with related cross sections obtained from a study of the visco-magnetic effect (Senftleben-Beenakker effect) in mixtures[5].

2. Theory. As discussed in chapter I, the correlation function C(t), determining the collisional broadening of the depolarized Rayleigh line of a gas consisting of linear molecules, has the general form:

$$C(t) = \frac{\sum_{\ell,m} < \frac{\overbrace{J_\ell J_\ell}}{J_\ell^{2} - \frac{3}{4}} (0) : \frac{\overbrace{J_m J_m}}{J_m^{2} - \frac{3}{4}} (t) >_0}{\sum_{\ell} < \frac{\overbrace{J_\ell J_\ell}}{J_\ell^{2} - \frac{3}{4}} (0) : \frac{\overbrace{J_\ell J_\ell}}{J_\ell^{2} - \frac{3}{4}} (0) >_0} \quad , \qquad (1)$$

where the brackets $< >_0$ indicate an equilibrium average and the indices ℓ and m label the molecules. This correlation function describes the decay of orientational fluctuations in the gas. For pure gases in the binary collision regime this decay can be associated with a cross section matrix $\underline{\underline{\sigma}}$ [6]:

$$C(t) = \frac{\sum_{i,j} p_j \, d_i d_j \, (e^{-n <v>_0 \, \underline{\underline{\sigma}} t})_{ij}}{\sum_j p_j \, d_j^{2}} \quad . \qquad (2)$$

The diagonal elements σ_{jj} determine the decay rate of the orientational polarization $\overbrace{\underline{J}\,\underline{J}}/(J^2 - \frac{3}{4})$ in rotational state j. The off-diagonal elements σ_{ij} describe the transfer of polarization from state j to state i. p_j is the fractional population of rotational state j, n the number density of the gas and $<v>_0$ the average relative velocity. The weighting factor d_j is given by

$$d_j = \left(\frac{J^2}{4J^2 - 3} \right)^{\frac{1}{2}} = \left[\frac{j(j+1)}{(2j-1)(2j+3)} \right]^{\frac{1}{2}} \quad . \qquad (3)$$

For mixtures of diatomic molecules with noble gas atoms, as studied here, the correlation function C(t) is again given by eq. (1). However, the expression for C(t) in terms of cross sections (eq. (2)) becomes more complicated. The destruction and transfer of orientational polarization of the (diatomic) molecules (species A, in our experiment N_2) is brought about not only by collisions between diatomic molecules, but also by collisions between diatomic molecules and noble gas atoms (species B). Hence two different cross section matrices are needed, denoted by $\underline{\underline{\sigma}}^{A}$ and $\underline{\underline{\sigma}}^{AB}$, describing the decay and transfer of polarization by A-A

collisions and A-B collisions, respectively. The correlation function for such a mixture takes the form:

$$C(t) = \frac{\sum_{i,j} p_j \, d_i d_j \, (e^{-[n_A \langle v_A \rangle_0 \underline{\underline{\sigma}}^A + n_B \langle v_{AB} \rangle_0 \underline{\underline{\sigma}}^{AB}]t})_{ij}}{\sum_j p_j \, d_j^2} \quad . \qquad (4)$$

The difference from the pure gas case is that the term $n \langle v \rangle_0 \underline{\underline{\sigma}}$ in the exponent of eq. (2) is now replaced by an expression linear in the number densities of both species, n_A and n_B. The average relative velocities are given by

$$\langle v_A \rangle_0 = \left(\frac{8 \, k_B T}{\pi \mu_A} \right)^{\frac{1}{2}} \quad \text{and} \quad \langle v_{AB} \rangle_0 = \left(\frac{8 \, k_B T}{\pi \mu_{AB}} \right)^{\frac{1}{2}} \quad , \qquad (5)$$

with μ_A and μ_{AB} reduced masses, while the other symbols have their usual meanings.

Two useful quantities to characterize the correlation function are the initial slope, describing the short time behavior, and the time integral, containing information on the behavior at all times. From eq. (4), the following relation for the initial slope $(dC/dt)_{t=0}$ is obtained:

$$-\left(\frac{dC}{dt}\right)_{t=0} = n_A \langle v_A \rangle_0 \frac{\sum_{i,j} p_j \, d_i d_j \, \sigma_{ij}^A}{\sum_j p_j \, d_j^2} + n_B \langle v_{AB} \rangle_0 \frac{\sum_{i,j} p_j \, d_i d_j \, \sigma_{ij}^{AB}}{\sum_j p_j \, d_j^2} \qquad (6)$$

As shown in chapter I (eq. 26)) one has:

$$\frac{\sum_{i,j} p_j \, d_i d_j \, \sigma_{ij}^A}{\sum_j p_j \, d_j^2} = \mathfrak{S}(0\hat{2})_A \quad , \qquad (7)$$

where $\mathfrak{S}(0\hat{2})_A$ is an effective cross section for the decay of orientational polarization in the pure gas. For the explicit expression for $\mathfrak{S}(0\hat{2})_A$ see chapter I. Analogously one has for the A-B collisions:

$$\frac{\sum_{i,j} p_j \, d_i d_j \, \sigma_{ij}^{AB}}{\sum_j p_j \, d_j^2} = \mathfrak{S}(0\hat{2})_{AB} \quad , \qquad (8)$$

with $\mathfrak{S}(0\hat{2})_{AB}$ being the effective cross section for the decay of the orientational polarization of A-molecules by A-B collisions. $\mathfrak{S}(0\hat{2})_{AB}$ is defined as

$$\mathfrak{S}(0\hat{2})_{AB} = \frac{1}{\langle v_{AB} \rangle_0} \frac{\langle \overbrace{\underline{J}\,\underline{J}}^{} / (J^2 - \tfrac{3}{4}) : R_0^{AB} \overbrace{\underline{J}\,\underline{J}}^{} / (J^2 - \tfrac{3}{4}) \rangle_0}{\langle \overbrace{\underline{J}\,\underline{J}}^{} / (J^2 - \tfrac{3}{4}) : \overbrace{\underline{J}\,\underline{J}}^{} / (J^2 - \tfrac{3}{4}) \rangle_0} \tag{9}$$

with the collision operator R_0^{AB} given by

$$R_0^{AB}\phi = -(2\pi)^4 \hbar^2 n_B^{-1} \, tr_B \int d\underline{p}_B \, f_B^{(0)} \{ \int t^{g_{AB}}_{g'_{AB}}(\phi') \, t^{g^{\dagger}_{AB}}_{g'_{AB}} \delta(E) \, d\underline{p}'_B - \\ - \frac{i}{2\pi} [t^{g_{AB}}_{g_{AB}}(\phi) - (\phi) \, t^{g^{\dagger}_{AB}}_{g_{AB}}] \} \, . \tag{10}$$

For the meaning of the various symbols see ref. 7.

Eq. (6) can now be written as

$$-\left(\frac{dC}{dt}\right)_{t=0} = n_A \langle v_A \rangle_0 \, \mathfrak{S}(0\hat{2})_A + n_B \langle v_{AB} \rangle_0 \, \mathfrak{S}(0\hat{2})_{AB} \, . \tag{11}$$

Thus the theory predicts that the initial slope of the correlation function depends linearly on the noble gas density n_B, with the proportionality constant characterized by the reorientation cross section $\mathfrak{S}(0\hat{2})_{AB}$.

The time integral of the correlation function, $\int_0^\infty C(t)\,dt$, which is a useful quantity for pure gases, does not have a simple interpretation for mixtures. The expression for this integral in terms of the cross section matrix elements, is a rather complicated function of the composition of the mixture (*cf.* eq. (4)). It cannot be broken up in a manner which will separate the contributions from different collision types. Therefore the time integral is only a useful quantity in the limit of infinite dilution of diatomic molecules in a bath of monatomics. The extrapolation to infinite dilution, however, is nonlinear and is experimentally only feasible when accurate data at relatively high noble gas concentration are available. For the present data, such an extrapolation proves to be of little use and therefore we will not discuss the time integral in the analysis of the experimental results.

3. Experimental results and discussion. Experiments have been performed on the systems N_2-He, N_2-Ne and N_2-Ar at 293 K. The experimental setup was identical to the one described in chapter I. For all mixtures, the N_2 density was kept fixed at 2.80 amagat and the depolarized Rayleigh line profile was measured at various noble gas densities. (Deviations from nonideality of the gases could be neglected). This method is similar to the one used by Jammu *et al.*[8] for the investigation of the noble gas broadening of rotational Raman lines.

The experimentally recorded spectra (interferograms) of the depolarized Rayleigh line have been corrected for various small spurious contributions which have been extensively discussed in chapter I. A Fourier transformation was applied to the interferograms after which the instrumental contribution to the spectral profile could be easily removed. As a result the Fourier transform $F_R(t)$ of the net depolarized Rayleigh line was obtained. This Fourier transform $F_R(t)$ is identified with the correlation function C(t) for the decay of orientational polarization in a mixture (see eq. (4)):

$$F_R(t) = C(t) \quad . \tag{12}$$

The experimental results for F_R as a function of time are given in figs. 1-3 for the systems N_2-He, N_2-Ne and N_2-Ar, respectively. The curves show deviations from simple exponential decay, indicating a non-Lorentzian lineshape. From the initial slope of the curves a quantity Γ is extracted, defined by

$$2\pi\Gamma = -\left(\frac{dF_R}{dt}\right)_{t=0} \quad . \tag{13}$$

Γ has the dimension of frequency. (For a Lorentzian line Γ would be identical to the half-width $\Delta\nu_{\frac{1}{2}}$, *i.e.*, half the width at half intensity.) In fig. 4 values for Γ are plotted as a function of the noble gas density $\rho_{n.g.}$ in amagat. The point at $\rho_{n.g.} = 0$ represents the value of Γ for pure N_2 at a density of 2.80 amagat. Within the experimental accuracy it is found that for all systems the dependence is linear, as predicted by theory (see eq. (11)). Using therefore the theoretical formulae as a

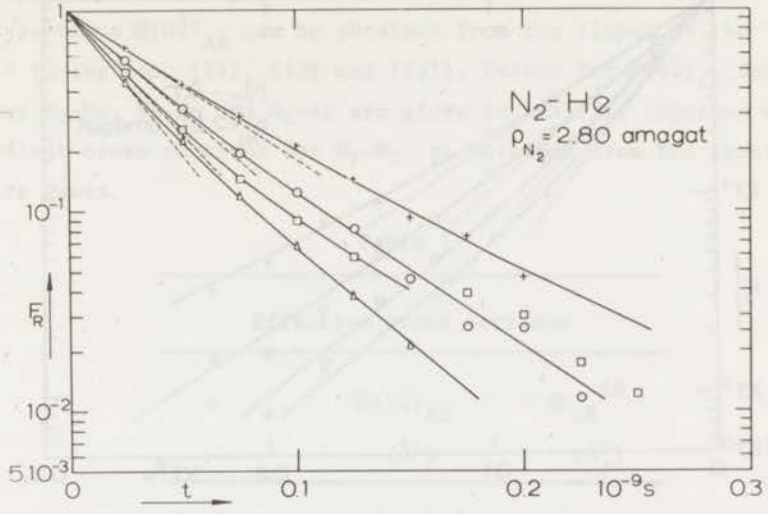

Fig. 1. F_R as a function of time for various H_2-He mixtures. ρ_{N_2} = 2.80 amagat.
+ ρ_{He} = 0 amagat, ○ ρ_{He} = 2.80 amagat, □ ρ_{He} = 4.66 amagat, △ ρ_{He} = 6.52 amagat.
The dashed lines correspond to the initial slopes of the curves.

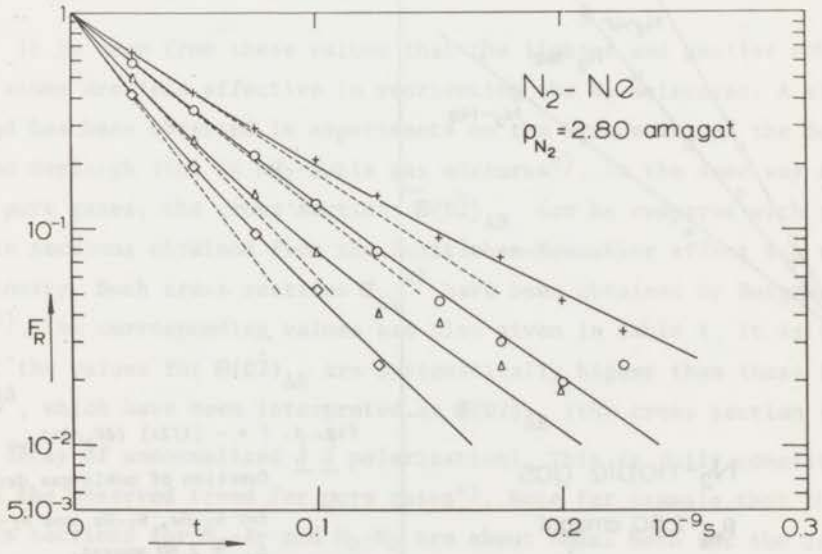

Fig. 2. F_R as a function for various N_2-Ne mixtures. ρ_{N_2} = 2.80 amagat.
+ ρ_{Ne} = 0 amagat, ○ ρ_{Ne} = 0.93 amagat, △ ρ_{Ne} = 2.80 amagat, ◇ ρ_{Ne} = 4.66 amagat.
The dashed lines correspond to the initial slopes of the curves.

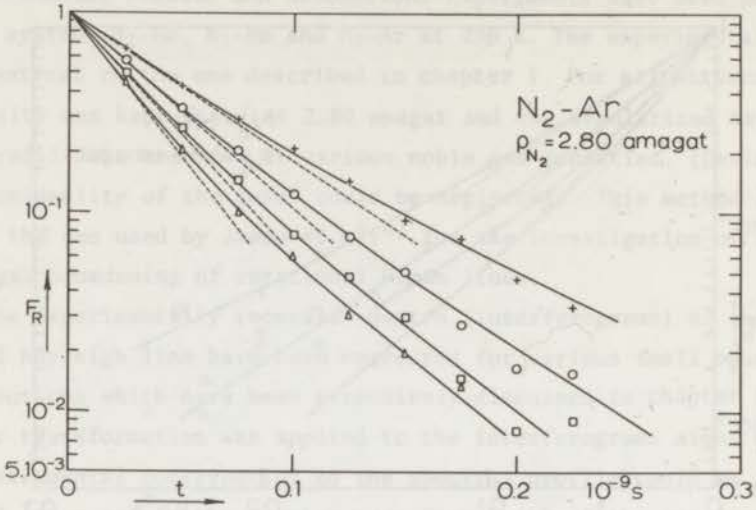

Fig. 3. F_R as a function of time for various N_2-Ar mixtures. ρ_{N_2} = 2.80 amagat. + ρ_{Ar} = 0 amagat, ○ ρ_{Ar} = 0.93 amagat, □ ρ_{Ar} = 1.86 amagat, △ ρ_{Ar} = 2.80 amagat. The dashed lines correspond to the initial slopes of the curves.

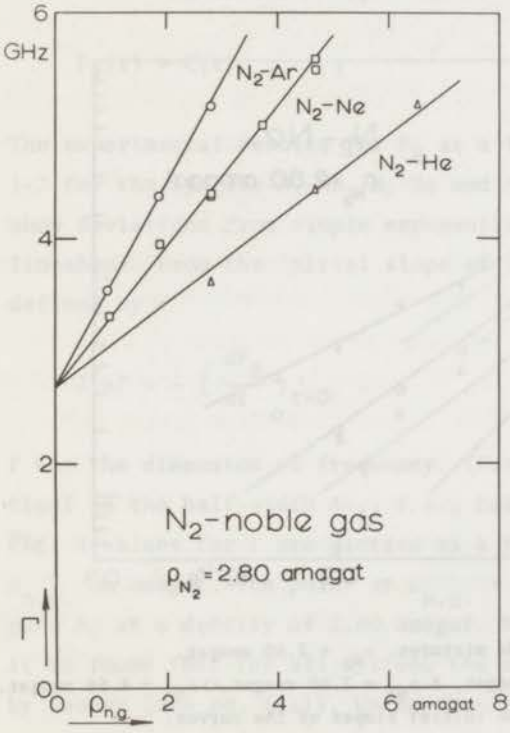

Fig. 4. $\Gamma = -(1/2\pi)(dF_R/dt)_{t=0}$ as a function of noble gas density for N_2-He, N_2-Ne and N_2-Ar. ρ_{N_2} = 2.80 amagat.

description for the experimental results*, values for the effective cross sections $\mathfrak{S}(0\hat{2})_{AB}$ can be obtained from the slopes of the lines in fig. 4 (using eqs. (11), (12) and (13)). Values for $\mathfrak{S}(0\hat{2})_{AB}$ for the systems N_2-He, N_2-Ne and N_2-Ar are given in table I, together with the equivalent cross sections for N_2-N_2, as obtained from the experiments on pure gases.

Table I

Effective cross sections

	$\mathfrak{S}(0\hat{2})_{AB}$ (Å^2)	$\mathfrak{S}_{SB}^{AB}$ (Å^2)
N_2-He	6.5 ± 0.7	5.6 ± 0.3
N_2-Ne	20 ± 2	15 ± 1
N_2-Ar	35 ± 3	24 ± 2
N_2-N_2	34.4 ± 0.6	23.7 ± 0.9

It is seen from these values that the lighter and smaller noble gas atoms are less effective in reorienting the N_2 molecules. A similar trend has been observed in experiments on the broadening of the depolarized Rayleigh line in nH_2-noble gas mixtures[9]. In the same way as for the pure gases, the cross sections $\mathfrak{S}(0\hat{2})_{AB}$ can be compared with related cross sections obtained from the Senftleben-Beenakker effect for the viscosity. Such cross sections $\mathfrak{S}_{SB}^{AB}$ have been obtained by Burgmans *et al.*[5]. The corresponding values are also given in table I. It is seen that the values for $\mathfrak{S}(0\hat{2})_{AB}$ are systematically higher than those for $\mathfrak{S}_{SB}^{AB}$, which have been interpreted as $\mathfrak{S}(02)_{AB}$ (the cross section for the decay of unnormalized $\overrightarrow{J\,J}$ polarization). This is fully consistent with the observed trend for pure gases[4]. Note for example, that the cross sections for N_2-Ar and N_2-N_2 are about equal both for the depo-

* Note that in chapter I the experimental cross section obtained from the initial slope of $F_R(t)$ has been introduced as $\mathfrak{S}_{DPR}$. At a later stage it has been identified with $\mathfrak{S}(0\hat{2})$.

larized Rayleigh and the Senftleben-Beenakker experiments, but that the difference between the two experiments is rather large. The conclusion given in chapter I that a description of the SB-effect for the viscosity in terms of the polarization $\overbrace{\underline{J}\,\underline{J}}/(J^2 - \frac{3}{4})$ is not appropriate, is therefore certainly also valid for N_2-noble gas mixtures.

References

1. Gordon, R.G., J. Chem. Phys. *44* (1966) 3083.
2. Hess, S., Z. Naturforsch. *24a* (1969) 1675; *25a* (1970) 350.
3. Hess, S., Springer Tracts Mod. Phys. *54* (1970) 136.
4. This thesis, chapter I; Keijser, R.A.J. *et al.*, Physica, to be published.
5. Burgmans, A.L.J., Van Ditzhuyzen, P.G. and Knaap, H.F.P., Z. Naturforsch. *28a* (1973) 849.
6. Shafer, R. and Gordon, R.G., J. Chem. Phys. *58* (1973) 5422.
7. Raum, H.H. and Köhler, W.E., Z. Naturforsch. *25a* (1970) 1178.
8. Jammu, K.S., St. John, G.E. and Welsh, H.L., Can. J. Phys. *44* (1966) 797.
9. Gupta, B.K. and May, A.D., Can. J. Phys. *50* (1972) 1747.

CHAPTER III

THE PRESSURE BROADENING OF THE ROTATIONAL RAMAN LINES OF THE HYDROGEN ISOTOPES

1. Introduction. In the spectrum of the light scattered from dilute gases consisting of linear molecules, a series of equidistant lines is observed at both sides of the elastically (Rayleigh) scattered light (see fig. 4 of the introduction to this thesis). These lines correspond to spectroscopic transitions between the rotational states of the molecules. The selection rules for such transitions are $\Delta j = j_f - j_i = \pm 2$, where j_i and j_f denote the initial and final states of a transition. The lines are known as the rotational Raman lines. The rotational Raman scattering as well as the depolarized Rayleigh scattering ($\Delta j = 0$) (discussed in chapters I[1]) and II[2]) originates from the anisotropic part of the molecular polarizability, $\alpha_{/\!/} - \alpha_{\perp}$.

From a study of the pressure or collisional broadening of the Raman lines information can be obtained about the different types of collision processes that occur between nonspherical molecules. Such information can be used for a determination of the nonspherical part of the intermolecular potential.

In the pressure broadening of rotational Raman lines both energetically inelastic and energetically elastic collisions play a role[3,4]). Inelastic collisions give rise to spectral line broadening because a change of j upon collision interrupts the radiation proces. The elastic effects are mainly due to collisional reorientation of the radiating molecules. A second elastic contribution, caused by the rotational phase shift in a collision, is generally much smaller. At not too high densities the pressure broadened Raman lines are well separated from each other and the line shape is Lorentzian. In this situation a study of the broadening of the lines with density provides information on the relevant collision processes as a function of the rotational quantum number j ($= j_i$).

Note that the situation for the depolarized Rayleigh line, although also originating from the anisotropic part of the polarizability, is essentially different. The broadening occurs as a result of molecular reorientation only (including also in this case the reorientation in inelastic collisions). Furthermore, all rotational states contribute to the depolarized Rayleigh line, which leads in general to a non-Lorentzian line shape[1].

In previous studies, both experimental[5] and theoretical[6,7], it was found that in general the widths of rotational Raman lines decrease with increasing j. This can simply be explained by the fact that for high j both energetically inelastic collisions and reorienting collisions become progressively less probable. Inelastic collisions are less probable at higher j because of the larger energy spacings between the rotational levels. That collisional reorientation becomes more difficult for molecules in higher rotational states is due to the increased gyroscopic stability, as has been discussed in chapter I.

It has been pointed out by Van Kranendonk[6] that a special case is formed by gases for which the energy spacings between the most populated rotational levels are large with respect to the average thermal energy. Since in such a situation inelastic collisions are infrequent, so-called resonance collisions may be relatively more important. In this type of collision the rotational energy changes of the radiating molecule and its collision partner exactly compensate each other, *i.e.*, there is no energy exchanged between rotational and translational degrees of freedom. While such resonance processes are not detected in studies of rotational relaxation by means of sound absorption experiments[8,9], in rotational Raman scattering their effect can indeed be observed. This has recently been indicated in studies on the broadening of HCl Raman lines[10-12].

A group of systems which seems very suitable to study such resonance collisions is formed by the hydrogen isotopes[6]. The energy level splitting is large and at room temperature only a few rotational levels are populated. Fig. 1 shows schematically the energy level diagram for H_2. For the homonuclear molecule H_2 (and also for D_2) transitions between ortho and para states are forbidden so that the smallest possible collisional jumps on the rotational ladder correspond to $\Delta j = \pm 2$. In HD, on

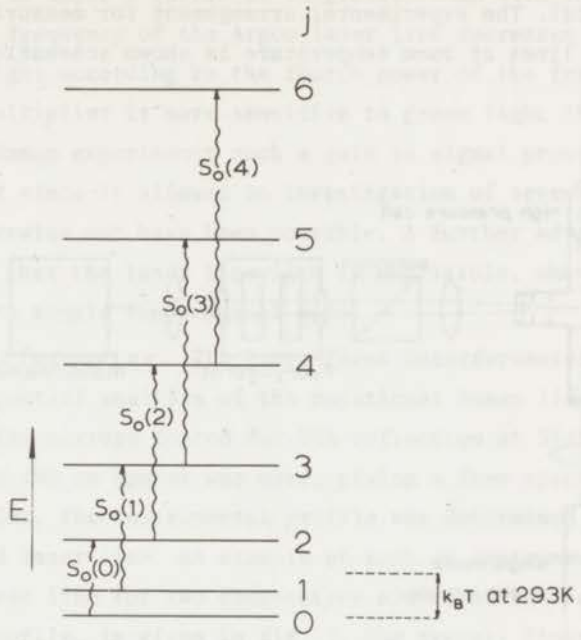

Fig. 1. Rotational energy level diagram for H_2 with Raman transitions.

the other hand, collisional transitions with $\Delta j = \pm 1$ are also allowed.

In order to investigate the collisional resonance effects we measured the pressure broadening of the rotational Raman lines in nH_2, HD and nD_2 at room temperature (293 K). For H_2 the linewidths have also been measured at various ortho-para compositions. Only the Stokes lines, corresponding to the spectroscopic transitions $\Delta j = j_f - j_i = +2$ were examined in detail. The anti-Stokes lines, which are much weaker, should show an identical behavior. In H_2 the lines $S_o(0)$ ($j = 0 \rightarrow j = 2$) through $S_o(4)$ ($j = 4 \rightarrow j = 6$) have been observed. In the pure rotational Raman spectrum the S refers to transitions with $\Delta j = +2$ (the subscript o indicates that only the lowest vibrational state is involved). The spectroscopic transitions for the investigated H_2 Raman lines have been indicated in fig. 1. Higher lines were too weak to be detected. In HD and nD_2 the pressure broadening was investigated for the lines $S_o(0)$ through $S_o(4)$ and $S_o(0)$ through $S_o(5)$, respectively. Preliminary results of this study have already been presented[13].

2. *Experimental.* The experimental arrangement for measuring the rotational Raman lines at room temperature is shown schematically in fig. 2.

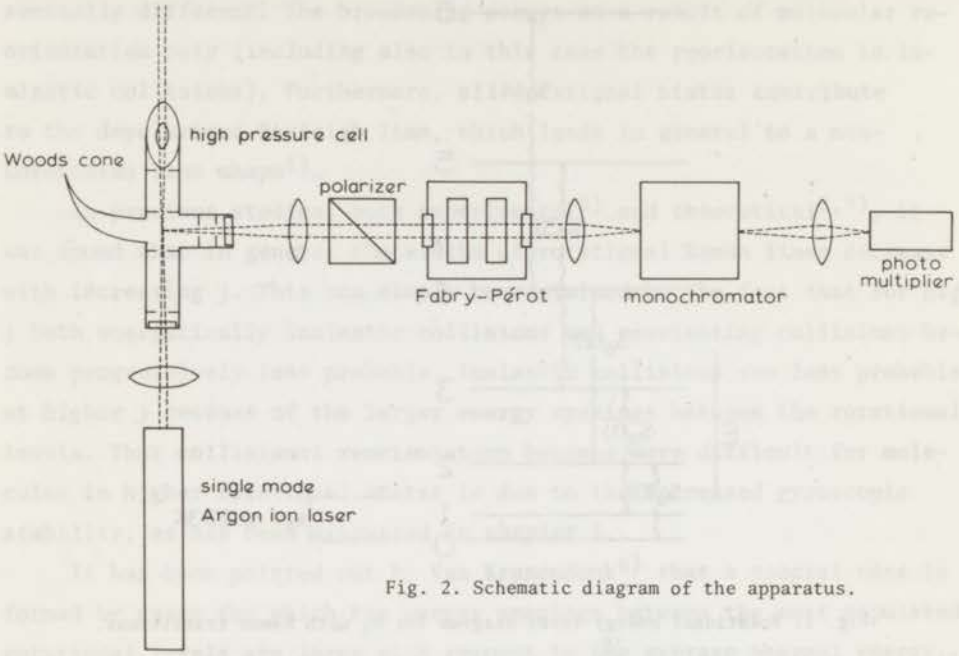

Fig. 2. Schematic diagram of the apparatus.

The beam of an Argon ion laser was focussed into a chamber which contained the sample gas at pressures up to 125 atm. The polarization of the light was vertical to the scattering plane. Scattered light was collected at right angles to the source. A small monochromator was utilized to isolate the region of the spectrum containing the individual Raman line of interest. This line was then spectrally analyzed with a pressure scanned Fabry-Pérot interferometer and standard photon counting equipment. As the setup is basically identical to the one used for the depolarized Rayleigh scattering experiments (chapter I), we discuss only the experimental details that are different from those described there.

2.1 Laser. A single (longitudinal) mode Argon ion laser (Spectra Physics model 165), operating at the green 5145 Å line, served as a light source. The advantage of the Argon laser over the 6328 Å He-Ne laser source, that was used in previous experiments[1,2], is the considerable gain in signal: (1) The optical power available with the Argon

laser (600 mW) is about a factor of 10 greater than with the He-Ne laser, (2) the higher frequency of the Argon laser line increases the amount of scattered light according to the fourth power of the frequency and (3) the photomultiplier is more sensitive to green light than to red light. In the Raman experiments such a gain in signal proved to be especially useful since it allowed an investigation of several weak lines, that would otherwise not have been possible. A further advantage of the Argon laser is that the laser linewidth is negligible, when the laser is operated in a single longitudinal mode.

2.2 Interferometer. The Fabry-Pérot interferometer that was used for the spectral analysis of the rotational Raman lines was equipped with two flat mirrors coated for 98% reflection at 5145 Å. For all experiments a 0.198 cm spacer was used, giving a free spectral range (FSR) of 75.6 GHz. The instrumental profile was determined by scanning the unbroadened laser line. An example of such an instrumental profile, showing the laser line for two consecutive orders of the Fabry-Pérot transmission profile, is given in fig. 3. The overall finesse is about 40. It is seen that the instrumental profile is somewhat asymmetric which is due to imperfect flatness of the interferometer mirror surfaces. The consequences of this will be discussed later. Another complication is the fact that the instrumental linewidth is slightly wavelength dependent in the spectral range of interest. This is mainly caused by the fact that

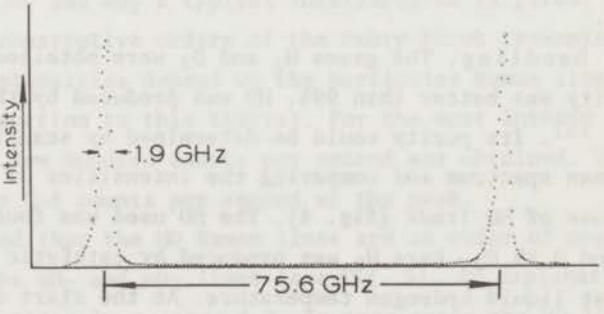

Fig. 3. Typical instrumental profile. Free spectral range (FSR): 75.6 GHz. Instrumental bandwidth: 1.9 GHz. Finesse (*i.e.*, the ratio of free spectral range and instrumental bandwidth): 40.

the reflectance of the interferometer mirrors decreases from 98% at 5145 Å to about 96.5% at 5500 Å. A correction for this effect - in most cases less than 1% - has been applied in the analysis of the experimental data.

2.3 Monochromator and polarizer. After transmission by the interferometer the light was focussed onto the entrance slit of a 25 cm Jarrel Ash monochromator (spectral slit width 6 Å or 15 Å), employed to isolate a particular Raman line in the spectrum of the scattered light. This isolation was essential since otherwise a severe overlapping of different orders of the Fabry-Pérot interferometer would have occurred in the spectral analysis. The use of a monochromator for this purpose is very convenient in this type of experiment, since it allows switching from one Raman line to another without realigning the optics. Using interference filters in such a situation is awkward since different lines require different filters.

The very strong polarized Rayleigh-Brillouin triplet was insufficiently rejected by the monochromator. Therefore it was decided to use a Glan-Thompson prism to eliminate the polarized spectrum. Consequently, only the depolarized component of the Raman spectrum was observed in the experiment. This does not affect the interpretation of the results since the pressure broadening of rotational Raman lines is known to be independent of the direction of polarization[14].

For further details of the setup and the experimental procedure see chapter I.

2.4 Gas handling. The gases H_2 and D_2 were obtained commercially. Their purity was better than 99%. HD was produced by the action of D_2O on $LiAlH_4$ [15]. Its purity could be determined by scanning the entire rotational Raman spectrum and comparing the intensities of H_2 and D_2 lines with those of HD lines (fig. 4). The HD used was found to contain about 3% H_2 and 0.5% D_2. Para H_2 was produced by catalytic conversion of normal H_2 at liquid hydrogen temperature. At the start of the experiments the para concentration was more than 96%. In the scattering cell, however, the pH_2 slowly converted back into nH_2. The conversion rate was sufficiently slow that measurements could be made as a function of ortho-para composition. For each experiment the ortho-para composition

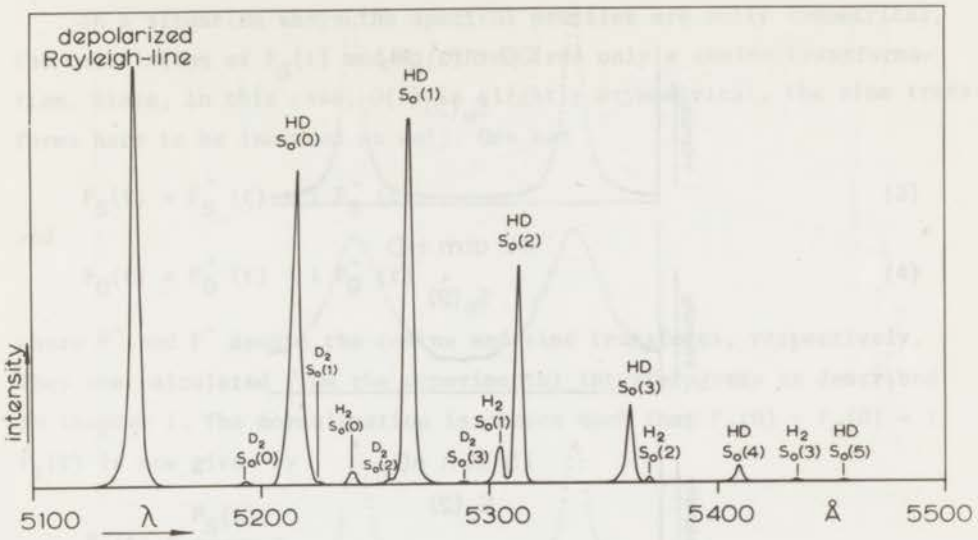

Fig. 4. Analysis of the isotopic purity of HD. The rotational Raman spectrum shows weak H_2 and D_2 lines. The intensity ratio of the various lines indicates that the sample contains 96.5% HD, 3% nH_2 and 0.5% nD_2.

could be determined within 2% by comparing the integrated intensities of odd and even lines.

3. Calculation of the results. Examples of experimental interferograms (spectra) of rotational Raman lines are shown in fig. 5. For each of the gases nH_2, HD and nD_2 a typical interferogram is given. The two peaks correspond to consecutive orders of the Fabry-Pérot transmission profile. The measured intensities depend on the particular Raman line investigated (see the introduction to this thesis). For the most intense lines a peak intensity of a few hundred counts per second was obtained. The weakest lines gave only 3-4 counts per second at the peak.

It is noted that the HD Raman lines are an order of magnitude broader than the nH_2 and nD_2 lines (see fig. 5). An explanation of this effect will be given in section 4.3. In some cases the HD lines were so broad that a fraction of the intensity in the far wings was cut off by the monochromator. A correction for this effect - at the most 3.5% of the total intensity of the line - has been applied. The interferograms

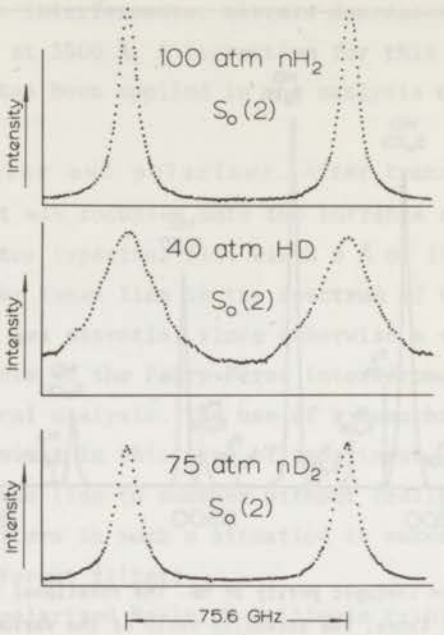

Fig. 5. Examples of Raman line interferograms.

were also corrected for the photomultiplier darkcount (typically 0.3 counts per second), which contributed to the spectrum as a flat background.

At this stage, an interferogram, described by a function $S(\nu)$ still contains the instrumental contribution. In fact $S(\nu)$ is a convolution of the true Raman line profile $R(\nu)$ with the periodic instrumental function $O(\nu)$:

$$S(\nu) = R(\nu) * O(\nu) = \int_{-\infty}^{+\infty} R(\nu')\, O(\nu - \nu')\, d\nu'. \qquad (1)$$

To separate the two contributions a Fourier transform technique is applied. The Fourier transforms of the functions in eq. (1) obey the relation

$$F_S(t) = F_R(t) \cdot F_O(t) \quad . \qquad (2)$$

$F_R(t)$, the transform of the net Raman line profile is now easily obtained once $F_S(t)$ and $F_O(t)$ have been determined from the experimental quantities $S(\nu)$ and $O(\nu)$.

In a situation where the spectral profiles are fully symmetrical, the calculation of $F_S(t)$ and $F_0(t)$ requires only a cosine transformation. Since, in this case, $O(\nu)$ is slightly asymmetrical, the sine transforms have to be included as well. One has

$$F_S(t) = F_S^+(t) + i\, F_S^-(t) \tag{3}$$

and

$$F_0(t) = F_0^+(t) + i\, F_0^-(t) \quad , \tag{4}$$

where F^+ and F^- denote the cosine and sine transforms, respectively. They are calculated from the experimental interferograms as described in chapter I. The normalization is chosen such that $F_S(0) = F_0(0) = 1$. $F_R(t)$ is now given by

$$F_R(t) = \frac{F_S(t)}{F_0(t)} =$$

$$\frac{F_S^+(t)F_0^+(t) + F_S^-(t)F_0^-(t)}{(F_0^+(t))^2 + (F_0^-(t))^2} + i\,\frac{F_S^-(t)F_0^+(t) - F_S^+(t)F_0^-(t)}{(F_0^+(t))^2 + (F_0^-(t))^2} \quad . \tag{5}$$

It was always found that the imaginary part of $F_R(t)$ was zero. The Raman line profiles are thus symmetrical, as should be the case. $F_R(t)$ is therefore calculated as the first term in eq. (5).

Typical results for F_R as a function of time for some Raman line profiles of the gases nH_2, HD and nD_2 are given in figs. 6-8. The semi-logarithmic plots show a linear behavior in all cases. $F_R(t)$ has thus a simple exponential form and can be written as

$$F_R(t) = e^{-2\pi\Delta\nu_{\frac{1}{2}}t} \quad , \tag{6}$$

where $\Delta\nu_{\frac{1}{2}}$ is the half-width (half the width at half intensity) of the associated Lorentzian line profile:

$$R(\nu) = \frac{I_0}{\pi}\,\frac{\Delta\nu_{\frac{1}{2}}}{\nu^2+\Delta\nu_{\frac{1}{2}}^2} \quad . \tag{7}$$

I_0 is the total integrated intensity of the Raman line and the central frequency of the line has been taken zero.

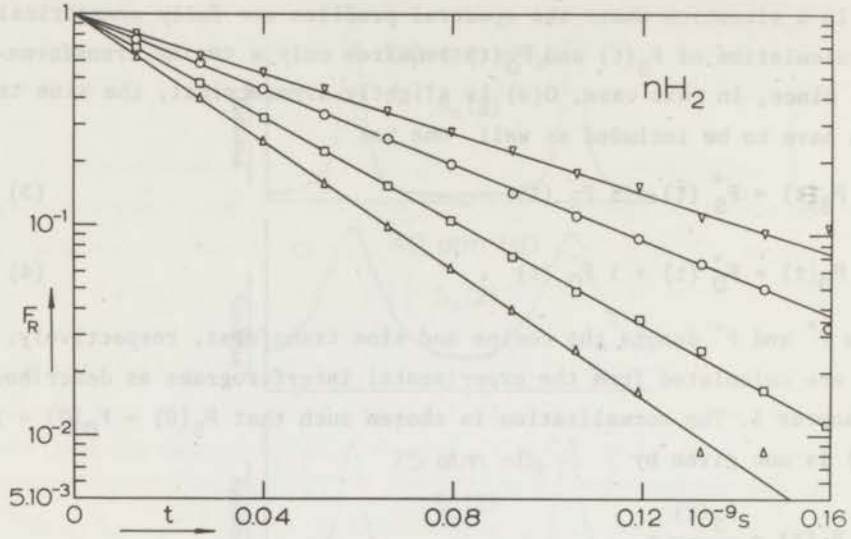

Fig. 6. F_R as a function of t for some rotational Raman lines of nH_2.
□ $S_o(0)$ 124.5 atm., △ $S_o(1)$ 124.5 atm., ○ $S_o(2)$ 100 atm., ▽ $S_o(4)$ 124.5 atm.

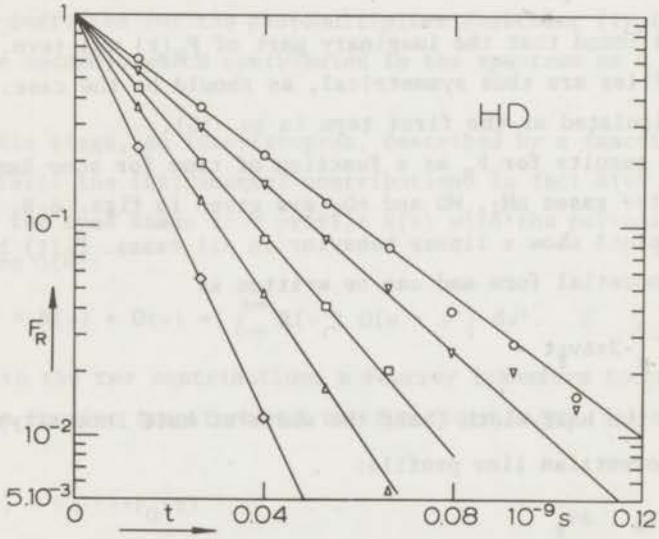

Fig. 7. F_R as a function of t for some rotational Raman lines of HD.
□ $S_o(0)$ 25 atm., ◇ $S_o(1)$ 50 atm., △ $S_o(2)$ 40 atm., ○ $S_o(3)$ 25 atm.,
▽ $S_o(4)$ 40 atm.

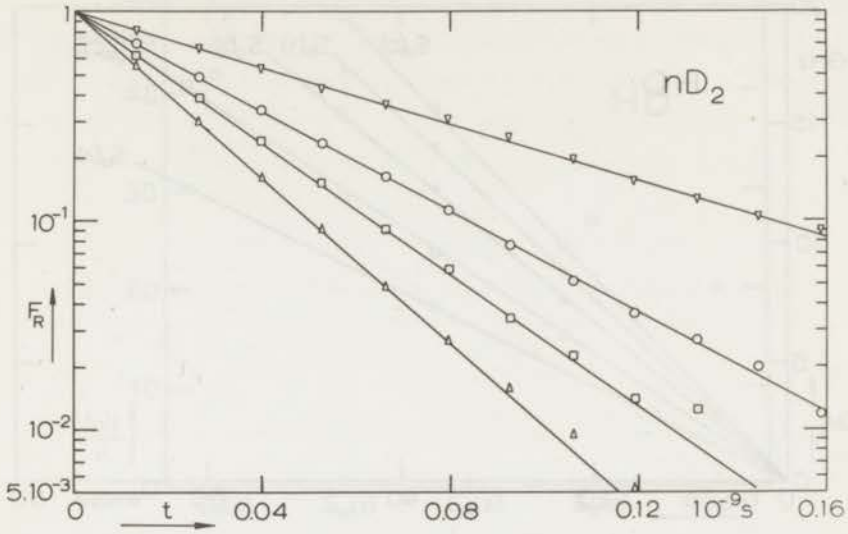

Fig. 8. F_R as a function of t for some rotational Raman lines of nD_2.
Δ $S_o(0)$ 100 atm., □ $S_o(1)$ 96 atm., ○ $S_o(3)$ 96 atm., ▽ $S_o(5)$ 96 atm.

The half-width $\Delta\nu_{\frac{1}{2}}$ is the characteristic parameter for the broadening of the Raman lines. It is easily determined from the plots of F_R *versus* t.

4. Experimental results and discussion. 4.1 HD, nH_2 and nD_2. Results are presented for the pressure broadened rotational Raman lines of HD, normal H_2 and normal D_2 at 293 K. Normal H_2 consists of 3/4 ortho (odd j) and 1/4 para (even j) and normal D_2 of 2/3 ortho (even j) and 1/3 para (odd j).

HD is discussed first, as the HD results follow the usual trend and have a simple explanation. The HD Raman lines have been investigated in the pressure range of 25-75 atm. The half-widths $\Delta\nu_{\frac{1}{2}}$ of the lines $S_o(0)$ through $S_o(4)$ are given in fig. 9 as a function of the density ρ. $\Delta\nu_{\frac{1}{2}}$ is found to be linear in the density, as should be expected*. Broadening

* The translational motion of the molecules gives rise to a contribution with a different density dependence. For the hydrogen isotopes this effect has been shown to be unimportant at pressures above 25 atm[16-18].

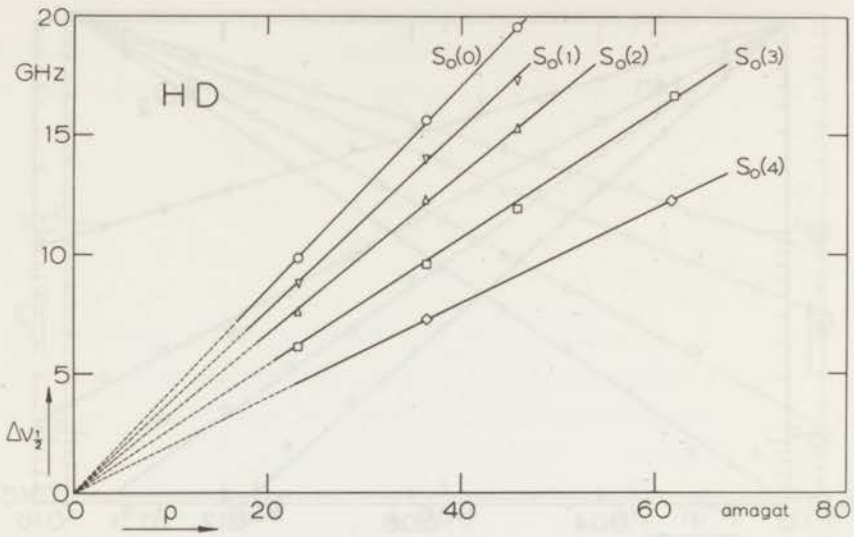

Fig. 9. $\Delta\nu_{\frac{1}{2}}$ as a function of ρ for the rotational Raman lines of HD.

Table I

Broadening coefficients of rotational Raman lines

	$\Delta\nu_{\frac{1}{2}}/\rho$ in GHz/amagat			
	HD	nH_2		nD_2
		this exp.	literature	
$S_o(0)$	0.43 ± 0.01	0.042 ± 0.001	0.042 ± 0.001 [a]	0.084 ± 0.001
$S_o(1)$	0.38 ± 0.01	0.052 ± 0.001	0.053 ± 0.001 [a]	0.067 ± 0.001
			0.054 ± 0.002 [b]	
$S_o(2)$	0.33 ± 0.01	0.037 ± 0.001	-	0.062 ± 0.001
$S_o(3)$	0.27 ± 0.01	0.038 ± 0.001	-	0.051 ± 0.001
$S_o(4)$	0.20 ± 0.01	0.023 ± 0.001	-	0.043 ± 0.001
$S_o(5)$	-	-	-	0.028 ± 0.001

A density of 1 amagat corresponds approximately to $2.687\ 10^{19}$ molecules/cm^3.

a) ref. 17.

b) ref. 18.

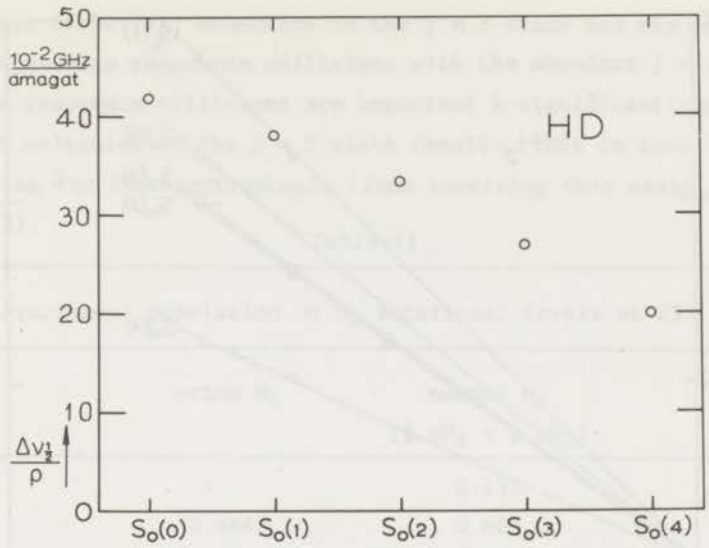

Fig. 10. $\Delta\nu_{\frac{1}{2}}/\rho$ for the rotational Raman lines of HD.

coefficients $\Delta\nu_{\frac{1}{2}}/\rho$ have been obtained from the slopes and are given in table I and fig. 10. It is seen that the broadening coefficients decrease smoothly with j. Such a monotonic decrease has also been found in pressure broadening studies of rotational Raman lines of larger molecules[5]. As pointed out in section 1 such a behavior is due to the fact that both inelastic and reorientation cross sections decrease with increasing j.

The Raman lines of nH_2 were investigated in the pressure range of 75-125 atm. The results for $\Delta\nu_{\frac{1}{2}}$ *versus* ρ are given in fig. 11. Values for $\Delta\nu_{\frac{1}{2}}/\rho$ are presented in table I and fig. 12. Previously obtained results for the broadening of the $S_0(0)$ and $S_0(1)$ lines are in excellent agreement with the present results.

The broadening coefficients $\Delta\nu_{\frac{1}{2}}/\rho$ for nH_2 show a behaviour that deviates markedly from the pattern found for HD. Instead of a regular decrease of the broadening with j, a distinct alternation is observed, the odd lines being relativly broader than the even ones.

This alternation of the broadening with j can be explained by the fact that resonance collisions play an important role in the broadening. In nH_2 at room temperature about 2/3 of the molecules are in the j = 1

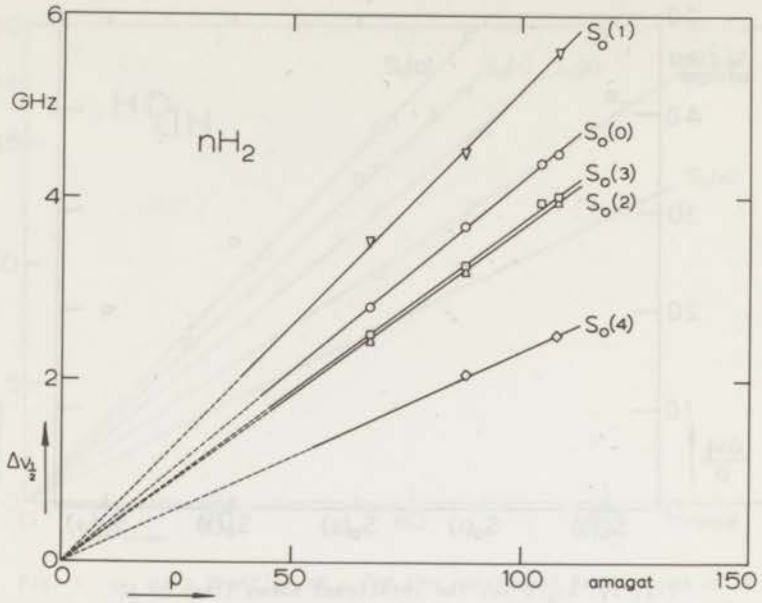

Fig. 11. $\Delta\nu_{\frac{1}{2}}$ as a function of ρ for the rotational Raman lines of nH_2.

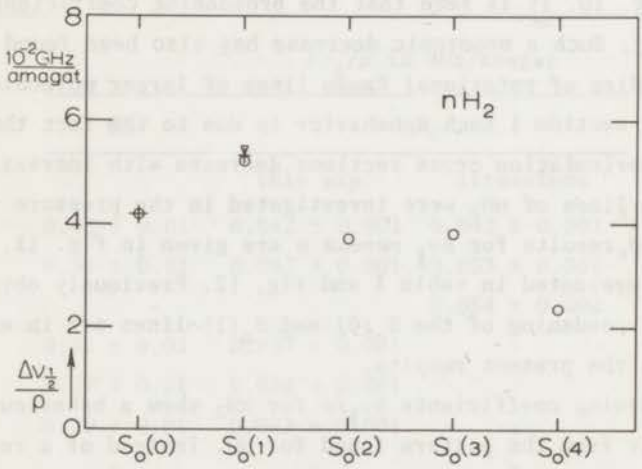

Fig. 12. $\Delta\nu_{\frac{1}{2}}/\rho$ for the rotational Raman lines of nH_2.
○ present results
+ Cooper *et al.*[17]
▽ Gupta and May[18]

state (see table II). Molecules in the j = 3 state are the only ones that can undergo resonance collisions with the abundant j = 1 molecules. If these resonance collisions are important a significantly shorter life time for molecules in the j = 3 state results. This in turn causes extra broadening for the spectroscopic lines involving this state, *viz.* $S_o(1)$ and $S_o(3)$.

Table II

Fractional population of H_2 rotational levels at 293 K

j	ortho H_2	normal H_2 ($\frac{3}{4}$ oH_2 + $\frac{1}{4}$ pH_2)	para H_2
0	-	0.132	0.525
1	0.884	0.662	-
2	-	0.115	0.460
3	0.115	0.086	-
4	-	0.004	0.015
5	0.001	0.001	-
6	-	0.000	0.000

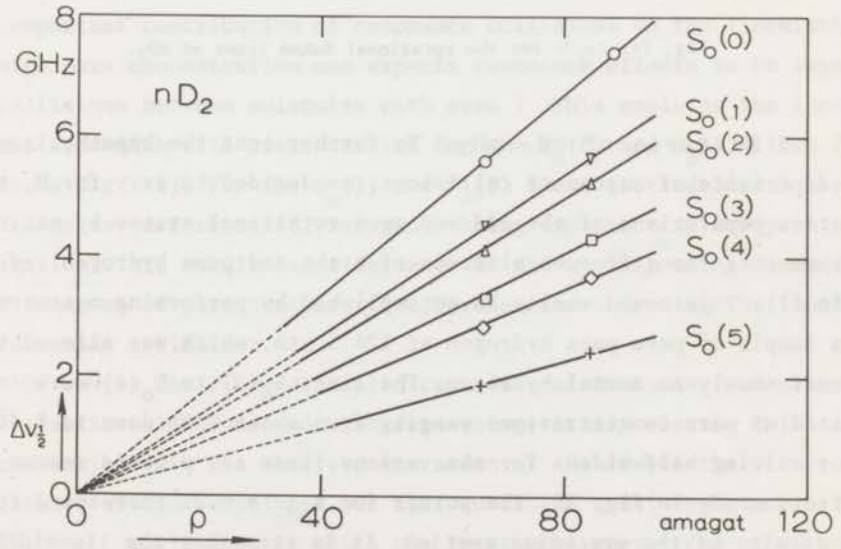

Fig. 13. $\Delta\nu_{\frac{1}{2}}$ as a function of ρ for the rotational Raman lines of nD_2.

The results for the Raman lines of nD_2 (see figs. 13 and 14 and table I) show a similar alternation in the broadening coefficients, although not as pronounced as in nH_2. The effect is here just opposite to that for nH_2, which is consistent with the reasoning above, since in nD_2 the even levels are more densely populated than the odd ones.

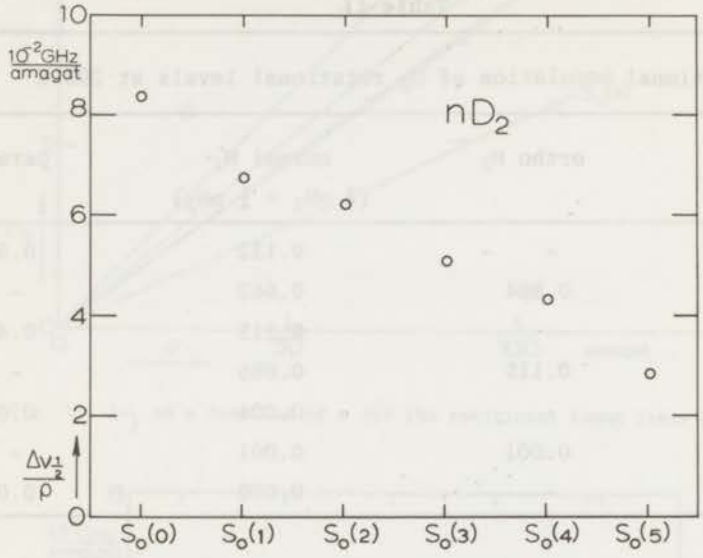

Fig. 14. $\Delta\nu_{\frac{1}{2}}/\rho$ for the rotational Raman lines of nD_2.

4.2 Mixtures of oH_2-pH_2. To further test the hypothesis of the importance of resonance collisions, we decided to vary for H_2 the relative populations of the odd and even rotational states by making measurements for different mixtures of ortho and para hydrogen (*cf.* table II). This could easily be accomplished by performing measurements on a sample of pure para hydrogen at 124.5 atm, which was allowed to convert slowly to normal hydrogen. The lines $S_o(0)$ to $S_o(4)$ were investigated at para concentrations ranging from about 0.96 down to 0.46. The resulting half-widths for the various lines are plotted *versus* concentration pH_2 in fig. 15. The points for $x_{pH_2} = 0.25$ correspond to the nH_2 results of the preceding section. It is seen that the linewidths for all lines vary linearly with concentration as should be expected

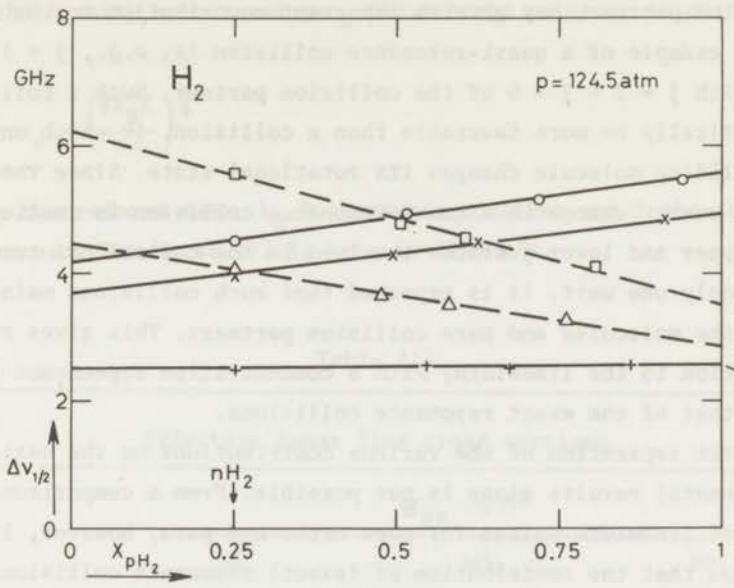

Fig. 15. The linewidths of the rotational Raman lines of H_2 as a function of ortho-para composition.

at a density where only binary collisions are important.

The different slopes for the various lines indicate very clearly the important contribution of resonance collisions to the linewidths. At high para concentration one expects resonance effects to be important in collisions between molecules with even j. This explains the increase of the linewidth with concentration for the $S_0(0)$ and $S_0(2)$ lines (solid lines in fig. 15). For the $S_0(1)$ and $S_0(3)$ lines (dotted lines) the situation is just reversed, resonance being important at low para concentration. This results in a decrease of the corresponding linewidths as a function of para concentration, further corroborating the importance of resonance collisions.

Of course the linewidths also contain contributions from other types of inelastic collisions and also from energetically elastic collisions. In connection with the observed variation of the linewidths with concentration it should be pointed out that so-called quasi-resonance collisions, *i.e.*, collisions in which the rotational energy change of one molecule is only partly compensated by the rotational energy change of

its collision partner, may give an important contribution to the linewidths. An example of a quasi-resonance collision is, *e.g.*, $j = 1 \rightarrow j = 3$ combined with $j = 2 \rightarrow j = 0$ of the collision partner. Such a collision may energetically be more favorable than a collision, in which only one of the colliding molecule changes its rotational state. Since the total rotational energy change in a quasi-resonance collision is smallest when both the upper and lower j states involved in the collisional transitions differ by only one unit, it is expected that such collisions mainly occur between ortho molecules and para collision partners. This gives rise to a contribution to the linewidths with a concentration dependence just opposite to that of the exact resonance collisions.

A direct separation of the various contributions on the basis of the experimental results alone is not possible. From a comparison of the extrapolated linewidth values for pure ortho and para, however, it can be concluded that the contribution of (exact) resonance collisions for some of the lines exceeds 40% of the total linewidth. The total contribution of resonance and quasi-resonance collisions is probably considerably higher. It can therefore be concluded that the angle-dependent part of the H_2 potential must contain an important term that allows for simultaneous transitions of collision partners, *e.g.*, the quadrupole-quadrupole interaction. A theoretical description for the broadening of the H_2 rotational Raman lines, based on such a quadrupole-quadrupole interaction, has been given by Van Kranendonk[6]. In section 5 we will compare our results with this theory.

4.3 Effective cross sections. It is often useful to express the experimental results in terms of effective cross sections, especially so since these are a better measure in the comparison of the results. Therefore we use the broadening coefficients and linewidths obtained in the preceding sections to calculate effective cross sections $\mathfrak{S}_{RR}$ with the relation

$$2\pi \, \Delta\nu_{\frac{1}{2}} = n \, \langle v \rangle_0 \, \mathfrak{S}_{RR} \quad . \tag{8}$$

n is the density number and $\langle v \rangle_0$ the average relative velocity, given by

$$\langle v \rangle_0 = \left(\frac{8 k_B T}{\pi \mu} \right)^{\frac{1}{2}} \qquad (9)$$

with μ the reduced mass, k_B Boltzmann's constant and T the absolute temperature. For H_2 at 293 K, $\langle v \rangle_0$ is 2485 m/s.

Table III

Effective Raman line cross sections

	$\mathfrak{S}_{RR}$ in Å^2		
	HD	nH_2	nD_2
$S_0(0)$	4.9 ± 0.1	0.40 ± 0.01	1.12 ± 0.01
$S_0(1)$	4.4 ± 0.1	0.49 ± 0.01	0.89 ± 0.01
$S_0(2)$	3.8 ± 0.1	0.35 ± 0.01	0.83 ± 0.01
$S_0(3)$	3.1 ± 0.1	0.36 ± 0.01	0.68 ± 0.01
$S_0(4)$	2.3 ± 0.1	0.22 ± 0.01	0.57 ± 0.01
$S_0(5)$	-	-	0.37 ± 0.01

Values for $\mathfrak{S}_{RR}$ for the rotational Raman lines of HD, nH_2 and nD_2 are presented in table III. A remarkable fact is that the effective cross sections for HD are an order of magnitude larger than those for nH_2 and nD_2. The cause of this lies in the asymmetric mass distribution in the HD molecule. This so-called loaded sphere character gives rise to a large P_1-term in the intermolecular potential. Such a P_1-type interaction leads to large inelastic collisional cross sections but does not allow simultaneous transitions of collision partners. The non-spherical part of the intermolecular potential for the homonuclear molecules H_2 and D_2 is much smaller as is also known from, *e.g.*, sound absorption experiments[19].

Using eq. (8) it is also possible to determine the effective cross sections $\mathfrak{S}_{RR}$ for the H_2 Raman lines in the limit of pure oH_2 and pure pH_2 from the extrapolated values of $\Delta\nu_{\frac{1}{2}}$ (fig. 15). The results are given in table IV.

Table IV

Effective Raman line cross sections in the limits of pure oH_2 and pH_2

	$\mathfrak{S}_{RR}$ in Å^2	
	oH_2	pH_2
$S_o(0)$	0.36 ± 0.01	0.49 ± 0.01
$S_o(1)$	0.54 ± 0.01	0.31 ± 0.01
$S_o(2)$	0.32 ± 0.01	0.43 ± 0.01
$S_o(3)$	0.39 ± 0.01	0.25 ± 0.01
$S_o(4)$	0.22 ± 0.01	0.23 ± 0.01

5. Comparison with theory. In order to understand the interpretation of the preceding section more quantitatively, the Raman line cross sections have been calculated using the impact theory of Fiutak and Van Kranendonk[20]. In particular the calculation of Van Kranendonk[6] is followed which uses a classical path description (straight line trajectories) for the translational states and neglects the spread in the velocities. For H_2 it assumes that the dominant term in the angle-dependent part of the intermolecular interaction is quadrupole-quadrupole. Other multipoles as well as induced intermolecular forces are neglected. The calculations have been carried out by Van Kranendonk for normal H_2 and we have extended these to obtain the Raman line cross sections for ortho and para H_2. This is simply accomplished by restricting the rotational averages over the perturbers to either even or odd parity. The calculations are carried out for the lines $S_o(0)$ through $S_o(4)$.

The results of these calculations for the various Raman lines are collected in table V. The contributions from different types of colli-

Table V

Effective Raman line cross sections for $\tau = \frac{d}{v} = 0.96\ 10^{-13}$ s

Cross sections in the limit of pure oH_2 (in $Å^2$)

	Elastic	Inelastic				$\mathfrak{S}_{RR}$	
		res.	quasi-res.	nonres. Δj_i or $\Delta j_f \neq 0$	nonres. $\Delta j_a \neq 0$	Total calc.	Exp.
$S_o(0)$	0.205	-	0.208	0.106	0.000	0.52	0.36
$S_o(1)$	0.248	0.287	0.001	0.000	0.000	0.54	0.54
$S_o(2)$	0.099	-	0.401	0.017	0.000	0.52	0.32
$S_o(3)$	0.056	0.285	0.003	0.000	0.000	0.34	0.39
$S_o(4)$	0.037	-	0.256	0.000	0.000	0.29	0.22

Cross sections in the limit of pure pH_2 (in $Å^2$)

	Elastic	Inelastic				$\mathfrak{S}_{RR}$	
		res.	quasi-res.	nonres. Δj_i or $\Delta j_f \neq 0$	nonres. $\Delta j_a \neq 0$	Total calc.	Exp.
$S_o(0)$	0.072	0.371	0.002	0.037	0.040	0.52	0.49
$S_o(1)$	0.087	-	0.353	0.000	0.049	0.49	0.31
$S_o(2)$	0.034	0.325	0.005	0.006	0.019	0.39	0.43
$S_o(3)$	0.020	-	0.375	0.000	0.011	0.41	0.25
$S_o(4)$	0.013	0.129	0.004	0.000	0.007	0.15	0.23

sions, *viz.* energetically elastic (reorientation), exact resonance, quasi-resonance and inelastic nonresonance, are listed separately. Inelastic nonresonance refers to collisions that are inelastic in only one of the colliding molecules, *i.e.*, either the radiating molecule (Δj_i or $\Delta j_f \neq 0$) or the perturber ($\Delta j_a \neq 0$). It can be seen from table V that for all lines a large fraction of the total broadening cross section is due to resonance and quasi-resonance contributions. All contributions are linear in the para concentration. The theoretical cross sections for the $S_o(1)$ and $S_o(3)$ Raman lines are compared with the ex-

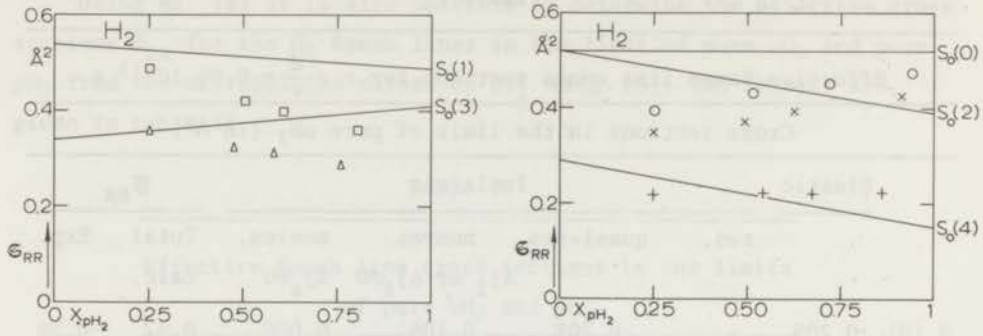

Fig. 16. Comparison between theory and experiment for the $S_0(1)$ and $S_0(3)$ Raman lines.
□ $S_0(1)$, Δ $S_0(3)$ experimental points
——— theory with $\tau = \frac{d}{v} = 0.96\ 10^{-13}$ s.

Fig. 17. Comparison between theory and experiment for the $S_0(0)$, $S_0(2)$ and $S_0(4)$ Raman lines.
○ $S_0(0)$, x $S_0(2)$, + $S_0(4)$ experimental points
——— theory with $\tau = \frac{d}{v} = 0.96\ 10^{-13}$ s.

perimental results in fig. 16. In fig. 17 the same is done for the $S_0(0)$, $S_0(2)$ and $S_0(4)$ lines. The distinct alternation in the slopes for the even and odd Raman lines, which is observed experimentally, is not reproduced by the theoretical calculations. This has to be attributed to an underestimate of the resonance collisions in the theory.

In Van Kranendonk's treatment the probability of a collision with an overall rotational energy change of $\hbar\omega$ is proportional to a resonance factor $g_0(\omega\tau)$, where τ measures the duration of the collision. This re-

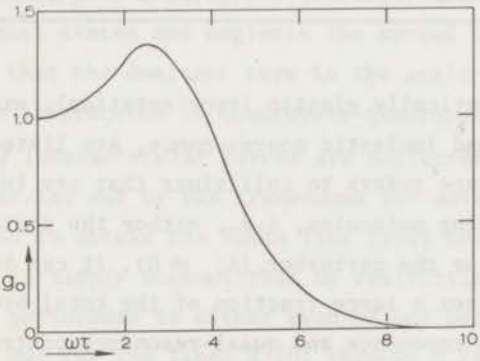

Fig. 18. The resonance factor $g_0(\omega\tau)$ for the quadrupole-quadrupole interaction (reproduced from ref. 6).

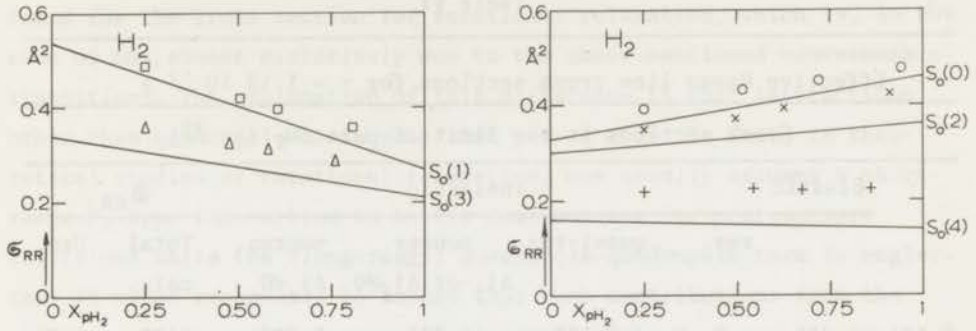

Fig. 19. Comparison between theory and experiment for the $S_0(1)$ and $S_0(3)$ Raman lines.
□ $S_0(1)$, Δ $S_0(3)$ experimental points
——— theory with $\tau = 1.18\ 10^{-13}$ s.

Fig. 20. Comparison between theory and experiment for the $S_0(0)$, $S_0(2)$ and $S_0(4)$ Raman lines.
○ $S_0(0)$, x $S_0(2)$, + $S_0(4)$ experimental points
——— theory with $\tau = 1.18\ 10^{-13}$ s.

sonance factor has for the quadrupole-quadrupole interaction the form shown in fig. 18 (which is taken from Van Kranendonk[6]). For exact resonance collisions one has $\omega = 0$ and $g_0(0) = 1$. For other inelastic collision processes, however, the value of $g_0(\omega\tau)$ and thus the collision probability, depends on τ. Different values of τ give a different weighting of such processes as compared to exact resonance collisions. Clearly any choice for τ would be an approximation as it is difficult to find a proper measure for the duration of a collision. Van Kranendonk approximated τ for impact parameters larger than the Lennard-Jones diameter d by $\tau = d/v$, with the relative velocity $v = (3k_BT/\mu)^{\frac{1}{2}}$. (Note that v has the same value for all collisions). This choice leads to poor agreement with experiment, as discussed above. It is found, however, that a slightly larger value for τ (about 20%), which is not unreasonable under the circumstances, changes the slopes of the lines as a function of para concentration drastically (see figs. 19 and 20 and table VI). The results are now in much better agreement with the experiment. It is seen from table VI that the contributions from quasi-resonance and nonresonance collisions are considerably smaller than for the original value of τ (*cf.* table V).

Table VI

Effective Raman line cross sections for $\tau = 1.18\ 10^{-12}$ s

Cross sections in the limit of pure oH_2 (in $Å^2$)

	Elastic	Inelastic				σ_{RR}	
		res.	quasi-res.	nonres. Δj_i or $\Delta j_f \neq 0$	nonres. $\Delta j_a \neq 0$	Total calc.	Exp.
$S_o(0)$	0.205	-	0.103	0.021	0.000	0.33	0.36
$S_o(1)$	0.248	0.287	0.000	0.000	0.000	0.54	0.54
$S_o(2)$	0.099	-	0.199	0.003	0.000	0.30	0.32
$S_o(3)$	0.056	0.285	0.000	0.000	0.000	0.34	0.39
$S_o(4)$	0.037	-	0.127	0.000	0.000	0.16	0.22

Cross sections in the limit of pure pH_2 (in $Å^2$)

	Elastic	Inelastic				σ_{RR}	
		res.	quasi-res.	nonres. Δj_i or $\Delta j_f \neq 0$	nonres. $\Delta j_a \neq 0$	Total calc.	Exp.
$S_o(0)$	0.072	0.371	0.000	0.007	0.008	0.46	0.49
$S_o(1)$	0.087	-	0.176	0.000	0.009	0.27	0.31
$S_o(2)$	0.034	0.325	0.000	0.001	0.004	0.36	0.43
$S_o(3)$	0.020	-	0.186	0.000	0.002	0.21	0.25
$S_o(4)$	0.013	0.129	0.000	0.000	0.001	0.14	0.23

From one point of view such a result, obtained from a simple theory by a slight modification of a rather uncertain parameter, may seem quite satisfactory. On the other hand, the very fact that the final results of the calculation are so sensitive to the choice of this parameter, indicates that a re-evaluation of the approximations in this theory is required.

Furthermore, in these calculations the contributions from inelastic nonresonance collisions in ortho H_2, *i.e.*, $j = 1 \rightarrow 3$ or $j = 3 \rightarrow 1$, are effectively zero (see table V and VI). On the other hand, in experiments on acoustical absorption in oH_2 [21] a value of 0.073 $Å^2$ is

found for the cross section for rotational relaxation, which is, in the case of oH_2, almost exclusively due to the above-mentioned nonresonance transitions. The explanation of this difference is that interactions other than quadrupole-quadrupole also play a role. In fact, in theoretical studies of rotational relaxation, one usually assumes a short-range P_2-type interaction to be the dominant one for nonresonance collisions while the (long-range) quadrupole-quadrupole term is neglected. It seems reasonable to assume that such contributions from the short range interactions cannot be ignored in the H_2 Raman line broadening.

Similar indications have been obtained from experiments on the pressure broadening of H_2 rotational Raman lines by noble gases[17,18,22]. In the H_2-noble gas interaction, the quadrupole-quadrupole term is obviously absent. Still the broadening of the H_2 Raman lines by noble gases is found to be only a factor 2 smaller than the self broadening, which strongly suggests that the self broadening cannot be attributed to quadrupole-quadrupole alone[17].

Recently calculations of the self broadening of the rotational Raman lines in H_2 based on a distorted wave Born approximation have been performed (private communication, ref. 23). A P_2-type of interaction is taken into account in addition to the quadrupole-quadrupole term. Satisfactory agreement with the results presented here is reported.

References.

1. This thesis, chapter I; Keijser, R.A.J. *et al.*, Physica, to be published.
2. This thesis, chapter II; Keijser, R.A.J. *et al.*, Physica, to be published.
3. Gordon, R.G., J. Chem. Phys. *44* (1966) 3083.
4. Shafer, R. and Gordon, R.G., J. Chem. Phys. *58* (1973) 5422.
5. Jammu, K.S., St. John, G.E. and Welsh, H.L., Can. J. Phys. *44* (1966) 797.
6. Van Kranendonk, J., Can. J. Phys. *41* (1963) 433.

7. Gray, C.G. and Van Kranendonk, J., Can. J. Phys. *44* (1966) 2411.
8. Sluijter, C.G., Knaap, H.F.P. and Beenakker, J.J.M., Physica *30* (1964) 745.
9. Jonkman, R.M., Prangsma, G.J., Keijser, R.A.J., Aziz, R.A. and Beenakker, J.J.M., Physica *38* (1968) 451.
10. Rich, N.H. and Welsh, H.L., Chem. Phys. Lett. *11* (1971) 292.
11. Fabre, D., Widenlocher, G. and Vu, H., Optics Commun. *4* (1972) 421.
12. Gray, C.G., Chem. Phys. Lett. *8* (1971) 527.
13. Keijser, R.A.J., Lombardi, J.R., Van Den Hout, K.D., De Groot, M., Sanctuary, B.C. and Knaap, H.F.P., Phys. Letters *45A* (1973) 3.
14. Gupta, B.K., Hess, S. and May, A.D., Can. J. Phys. *50* (1972) 778.
15. Fookson, A., Pomerantz, P. and Rich, E.H., J. Res. Natl. Bur. Std. *47* (1951) 31.
16. Cooper, V.G., May, A.D., Hara, E.H. and Knaap, H.F.P., Can. J. Phys. *46* (1968) 2019.
17. Cooper, V.G., May, A.D. and Gupta, B.K., Can. J. Phys. *48* (1970) 725.
18. Gupta, B.K. and May, A.D., Can. J. Phys. *50* (1972) 1747.
19. Prangsma, G.J., Heemskerk, J.P.J., Knaap, H.F.P. and Beenakker, J.J.M., Physica *50* (1970) 433.
20. Fiutak, J. and Van Kranendonk, J., Can. J. Phys. *40* (1962) 1085; *41* (1963) 21.
21. Prangsma, G.J., Borsboom, L.J.M., Knaap, H.F.P., Van Den Meijdenberg, C.J.N. and Beenakker, J.J.M., Physica *61* (1972) 527.
22. May, A.D., Degen, V., Stryland, J.C. and Welsh, H.L., Can. J. Phys. *39* (1961) 1769.
23. Moraal, H., Physica, to be published.

SAMENVATTING

In dit proefschrift worden experimenten beschreven betreffende de drukverbreding van de gedepolariseerde Rayleighlijn en de rotatie Ramanlijnen in het lichtverstrooiingsspectrum van gassen bestaande uit lineaire moleculen. Zoals bekend hangt deze lijnverbreding samen met de verstoring van de interne toestanden van de moleculen door botsingen. Voor de gedepolariseerde Rayleighlijn zijn daarbij uitsluitend veranderingen in de richting van het impulsmoment $\underline{J}$ van belang (reorientatie). Bij de rotatie Ramanlijnen spelen echter ook veranderingen in de absolute grootte van $\underline{J}$ (inelastische botsingsovergangen) een belangrijke rol.

Langs deze weg wordt directe informatie verkregen over verschillende soorten botsingsprocessen. Deze informatie kan worden gebruikt voor het testen van theoretische modellen voor de beschrijving van het hoekafhankelijke deel van de intermoleculaire wisselwerking.

Bij de lichtverstrooiingsexperimenten is gebruik gemaakt van een He-Ne laser en in een later stadium van een Argon ionen laser. In hoofdstuk I wordt een beschrijving gegeven van de gebruikte meetmethode. Hierna worden de resultaten gepresenteerd van metingen aan de gedepolariseerde Rayleighlijn voor de gassen, nH_2, pH_2, HD, nD_2, N_2, CO, CO_2 en OCS (bij 293 K). Aangetoond wordt dat voor het merendeel der onderzochte gassen afwijkingen optreden van de tot nu toe als algemeen geldend aangenomen Lorentzvorm. Dit effect wordt toegeschreven aan het feit dat de reorientatiekans van een molecuul afhangt van zijn rotatietoestand. De resultaten worden bediscussieerd aan de hand van een drietal theoretische modellen. Ook wordt een vergelijking gemaakt met de uitkomsten van studies van kernspinrelaxatie (NMR) en van metingen aan het Senftleben-Beenakker (SB) effect voor de viscositeit, welke experimenten eveneens informatie verschaffen over botsingsreorientatie van moleculen. Bij deze vergelijking ligt het accent op de verschillen die er tussen de resultaten van de diverse experimenten bestaan.

In hoofdstuk II worden de resultaten gegeven van een onderzoek naar de verbreding van de gedepolariseerde Rayleighlijn van N_2 in mengsels met edelgassen. Deze uitbreiding van de experimenten naar mengsels is

vooral van belang vanwege de relatief eenvoudige theoretische beschrijving van het botsingsproces tussen een twee-atomig molecuul en een edelgasatoom.

Een onderzoek naar de verbreding van rotatie Ramanlijnen is uitgevoerd voor de gassen nH_2, HD en nD_2. Voor H_2 is ook het gedrag als functie van de ortho-para samenstelling onderzocht. De resultaten van deze metingen worden in hoofdstuk III beschreven. Voor HD blijkt de verbreding van de Ramanlijnen met toenemend rotatiequantumgetal j op de gebruikelijke manier af te nemen. Bij nH_2 en nD_2 wordt echter een alternering in de breedtes waargenomen. Uit de resultaten voor oH_2-pH_2 mengsels blijkt dat dit effect toegeschreven moet worden aan het optreden van resonante botsingen. Dit zijn inelastische botsingen waarbij de rotatie-energie afgestaan door het ene molecuul precies gelijk is aan de rotatie-energie opgenomen door zijn botsingspartner. Aangetoond wordt dat de bestaande theorie geen bevredigende beschrijving geeft van het experimenteel gevonden gedrag.

Op verzoek van de faculteit der Wiskunde en Natuurwetenschappen volgen hier enige gegevens over mijn studie.

Na mijn Gymnasium-β opleiding van 1956 tot 1962 aan het Sint Janscollege te 's-Gravenhage begon ik in september 1962 mijn studie aan de Rijksuniversiteit te Leiden, waar ik in 1965 het kandidaatsexamen Natuurkunde en Wiskunde met bijvak Sterrenkunde aflegde. Sindsdien ben ik werkzaam op het Kamerlingh Onnes Laboratorium in de werkgroep voor Molecuulfysica onder leiding van Prof. Dr. J.J.M. Beenakker en Dr. H.F.P. Knaap. Tot mijn doctoraalexamen werkte ik mee aan een onderzoek naar rotatie-translatie relaxatie in verdunde gassen. In 1968 legde ik het doctoraalexamen experimentele natuurkunde af en begon ik aan het in dit proefschrift beschreven onderzoek. Sinds 1968 ben ik als wetenschappelijk medewerker in dienst van de Stichting voor Fundamenteel Onderzoek der Materie (F.O.M.). Vanaf 1966 ben ik als assistent betrokken geweest bij het natuurkunde-onderricht aan pre-kandidaten.

In 1966 was ik gedurende twee maanden werkzaam in het "Instituut voor Lage Temperaturen en Technische Fysica" in Leuven. In 1969 werd mij een beurs toegekend voor een stage van drie maanden in het IBM Research Center in Houston.

Velen hebben een bijdrage geleverd aan het tot stand komen van dit proefschrift. Bij het van de grond komen van het onderzoek is de expertise en daadwerkelijke steun van het Physics Department van de Universiteit van Toronto en met name van Prof. A.D. May van grote betekenis geweest. Ook de inbreng van Dr. V.G. Cooper, Dr. R.M. Jonkman en Drs. F. Baas in deze moeilijke beginfase mag niet onvermeld blijven. In een later stadium van het experimentele werk werd ik geassisteerd door Drs. M.A. Jansen, Drs. K.D. van den Hout, M. de Groot en R.E. Beekman. Voorts zij gememoreerd de stimulerende invloed van Prof. C.M. Knobler en Prof. J.R. Lombardi, die beiden gedurende een jaar zeer nauw bij het onderzoek betrokken zijn geweest.

Verder gaat mijn dank naar Dr. S. Hess voor zijn voortdurende interesse en diverse suggesties. Ook de belangstelling van Prof. R.G. Gordon, Prof. F.R. McCourt en Dr. H. Moraal is een belangrijke stimulans

geweest. De discussies met Prof. J.J.M. Beenakker, Prof. R.F. Snider en Dr. B.C. Sanctuary hebben veel bijgedragen tot een beter inzicht in de achtergronden van het onderzoek.

Ook aan de technische staf van het Kamerlingh Onnes Laboratorium ben ik veel dank verschuldigd. De constructie van de voor het onderzoek benodigde apparatuur werd op bekwame wijze uitgevoerd door de heren J.M. Verbeek, P. Zwanenburg, H. van Zanten, P.J.M. Vreeburg en J. Turenhout. Een aantal onmisbare voorzieningen kwam tot stand dank zij de inspanning van velen, van wie ik hier met name de heren C. le Pair en H. Kossen wil noemen.

Mejuffrouw A.M. Aschoff ben ik zeer erkentelijk voor het typen van het manuscript. Het tekenwerk werd verricht door de heer W.J. Brokaar, terwijl de heer W.F. Tegelaar voor de foto's zorgde.